

# A novel characterization of structures in smooth regression curves: from a viewpoint of persistent homology

Satish Kumar

IIT Kanpur

Department of Mathematics and Statistics

Kanpur 208016, India

Email: satsh@iitk.ac.in

Subhra Sankar Dhar

IIT Kanpur

Department of Mathematics and Statistics

Kanpur 208106, India

Email: subhra@iitk.ac.in

January 14, 2025

## Abstract

We characterize structures such as monotonicity, convexity, and modality in smooth regression curves using persistent homology. Persistent homology is a key tool in topological data analysis that detects higher dimensional topological features such as connected components and holes (cycles or loops) in the data. In other words, persistent homology is a multiscale version of homology that characterizes sets based on the connected components and holes. We use super-level sets of functions to extract geometric features via persistent homology. In particular, we explore structures in regression curves via the persistent homology of super-level sets of a function, where the function of interest is - the first derivative of the regression function.

In the course of this study, we extend an existing procedure of estimating the persistent homology for the first derivative of a regression function and establish its consistency. Moreover, as an application of the proposed methodology, we demonstrate that the persistent homology

of the derivative of a function can reveal hidden structures in the function that are not visible from the persistent homology of the function itself. In particular, we characterize structures such as monotonicity, convexity, and modality, and propose a measure of statistical significance to infer these structures in practice. Finally, we conduct an empirical study to implement the proposed methodology on simulated and real data sets and compare the derived results with an existing methodology.

## 1 Introduction

The shape of the regression function plays a crucial role in postulating the hypothesis about the regression model. One of the ways of characterizing the shape of a function is, by using derivatives of the function. Derivatives of a function provide important information about the shape of the function such as monotonicity, convexity, critical points, inflection points, etc. Therefore, to gain insights into the shape of the regression function from the observed data, one can estimate the derivatives and use them to infer global geometric features of the underlying true regression function. One such way of estimating the derivative is, by estimating the regression function from suitable smoothing techniques for example; the Nadaraya-Watson estimator, and then taking its derivative. There are various ways of estimating derivatives of a regression function (see, e.g., [24], [17], [16]). However, we use the derivative of the Nadaraya-Watson estimator as an estimate of the derivative of the regression function.

There have been various attempts to explore the shape of the regression function from the geometric perspective, for instance; [28] proposed a rank correlation coefficient to compare the shape of regression functions. In a different line of approach, motivated by the scale-space view from computer vision literature, [6] proposed a graphical device called SiZer to explore structures, such as peaks and valleys, in regression curves. SiZer analysis has been used in comparing two or more regression curves (see, e.g., [33], [32]). [18] proposed a graphical device, based on the derivative and inverse of the derivative of the regression function, to compare the two regression functions up to shift in the horizontal and/or vertical axis. [20] compared the time-varying quantile regression curves up to the horizontal shift.

However, unlike aforesaid works, we explore the shape of the regression function from the topological perspective. In particular, we attempt to describe the shape of the regression function in terms of connected components and holes, using the persistent homology (see, e.g., [21], [25]). One of the advantages of using topological features to describe the shape of a function is that these features provide qualitative global geometric information about the data, and are stable under deformations. Hence, statistical inference based on these topological features, such as connected components and holes, is robust to various deformations in the data (see, e.g., [3], [4], [5]).

Now, let  $f$  be a real-valued function. Then for a given  $t \in \mathbb{R}$ , the super-level set of  $f$  at the level  $t$  is defined as

$$D_t \triangleq \{x \in \mathbb{R} : f(x) \geq t\}. \quad (1.1)$$

The set  $D_t$  contains important structural information about the function  $f$ , and therefore, is a fundamental object to analyze in many statistical procedures. For instance, [26] defines the number of clusters in a statistical population as the number of connected components of  $D_t$ , where the underlying function is the probability density function. [30] proposed a test of multimodality of the probability density function based on the super-level sets. There is a vast literature on level-set estimation (see, e.g., [14], [36]), and numerous applications of super-level sets in statistical procedures (see, e.g., [13], [19], [15]).

We analyze super-level sets of a function from a topological perspective. In particular, we take the function to be analyzed as the first derivative of the regression function and then calculate the persistent homology of its super-level sets. Since the regression function is usually not known in practice, we estimate the persistent homology using an estimate of the derivative of the regression function. In this paper, we take the derivative of the Nadaraya-Watson estimator as an estimator of the derivative of the regression function. The validity of such estimators of persistent homology is due to the well-known stability theorem (see [11]). The stability theorem provides an upper bound of the bottleneck distance between true persistent homology and the estimated persistent homology in terms of the sup-norm distance between the underlying function and the corresponding estimator. Thus, if the estimator of the underlying function is uniformly convergent, then the corresponding persistent homology is consistent with respect to

the bottleneck metric.

However, in the present context, we do not have any estimator of the derivative of the regression function, which is uniformly convergent. To circumvent this issue, we adopt the procedure proposed by [1] to estimate the persistent homology. This procedure is applied in a particular case where the estimator of the underlying functions is based on kernel estimation and the underlying functions are taken to be either density functions or regression functions. [1] established the consistency of the proposed procedure up to the precision of  $5\epsilon$ , where  $\epsilon$  is any positive number involved in controlling topological features. The main advantage of this procedure is that it does not require uniform consistency of the estimator of the underlying function for the stability of the estimator of persistent homology.

## 1.1 Our contribution

The persistent homology of a function does not reveal local geometric features of its own accord. It only reveals global topological features such as connected components and holes in higher dimensions. It is worth mentioning here that the use of persistent homology to study the geometric structures of 1-manifolds is mainly limited to the clustering structures. The use of persistent homology to infer local geometric structures is not so straightforward, and such procedures have been less developed in the literature. In this work, we study the local geometric features such as monotonicity, convexity, and modality of smooth regression functions not by studying their persistent homology but by exploring the persistent homology of their derivative. The methodology adopted here appears analogous to the procedure proposed by [1] to estimate the persistent homology of the derivative of the regression function, though they are entirely different too. In the present work, the goal is not only to recover the persistent homology of the true function but also to infer local geometric features of the underlying function using persistent homology. In contrast, the goal in [1] is to devise a new procedure to infer the persistent homology of density and regression functions. [1] established consistency of the proposed estimator of persistent homology for density and regression functions using their kernel estimators. In a complementary fashion, we extend those results to the first derivative

of the regression function and establish consistency of the estimator of persistent homology up to the precision  $5\epsilon$ .

As an application of the proposed procedure, we demonstrate that it can be used to study the shape of regression functions. In particular, we characterize structures such as monotonicity, convexity, and modality in smooth regression curves and propose a measure of the statistical significance of these structures observed in the data. Moreover, one can adopt the proposed procedure to compare or cluster analysis of regression curves based on these structures. One of the real-life applications of our work is that given the regression curves of population growth of different subcontinents, one can investigate the shape of the first derivative of regression functions to compare the population growth patterns over time.

## 1.2 Mathematical challenges

Most of the techniques in the literature first obtain an estimator of the underlying function converging uniformly to its population counterpart and then use this estimator to estimate the persistent homology. As mentioned previously such procedures are supported by the stability results for persistent homology (see, Theorem 2.1).

There are various methods for estimating the derivative of the regression function but we are not aware of any result that establishes uniform consistency of the estimator. Therefore, most of the existing methods of estimating the persistent homology are ruled out in this case. To fix this, we use the procedure proposed by [1] to estimate the persistent homology of the derivative of the regression function.

The main problem with extending these results to the derivative of the regression function is the lack of estimation procedures that estimate the derivative directly from the observed data and have strong consistency properties. Therefore, we first estimate the regression function by the Nadaraya-Watson estimator assuming the regularity conditions under which it is strongly consistent, then take the first derivative of this estimator as the estimate of the first derivative of the regression function. We restrict our analysis only up to the first derivative of the regression function due to the complex form of the estimator which makes calculation intractable. Even

with the first derivative due to the complex form of the estimator, it is not feasible to use Bernstein’s inequality while calculating the false positive and false negative error of the set  $\{X_i : \hat{f}_n(X_i) \geq t, i = 1, \dots, n\}$  with respect to  $D_t$  (see, Equation 1.1), where  $X_i$ ’s are observed data, and  $\hat{f}_n$  is a kernel estimator of the underlying function  $f$ . Therefore we use Hoeffding’s inequality which provides less sharp bounds than Bernstein’s inequality which has been used in [1].

### 1.3 Outline

The rest of the article is organized as follows. Section 2 gives the necessary topological background to elaborate the notion of persistent homology. Section 3 formulates the exact problem and the main results of the article. Section 5 presents some applications of the proposed methodology. Section 7 consists of some concluding remarks. Finally, proofs of the main theoretical results are supplied in the appendix.

## 2 Preliminaries

Persistent homology (see, e.g., [21], [25], [37]) is a prominent tool in topological data analysis (TDA) that provides a multi-scale summary of topological features present in the data. Persistent homology is a multiscale extension of homology which is one of the refined topological invariants from algebraic topology (see; e.g., [29], [27]). Heuristically, homology characterizes sets based on the number of connected components and holes using some algebraic machinery. In what follows, we are concerned with the homology of simplicial complexes referred to as simplicial homology. Simplicial complexes are combinatorial representations of topological spaces made up of points, lines, edges, triangles, and their higher dimensional analogs. In the following subsections, we briefly describe the necessary background and definitions related to the algebraic topology.

## 2.1 Simplicial homology

In this subsection, we define the procedure to compute the homology of simplicial complexes. Note that given a finite set of points in a Euclidean space, one can geometrically define simplicial complexes (see, e.g., [29], [27]). However, in TDA, data points may not be embedded into the Euclidean spaces, therefore one works with the abstract simplicial complexes. In what follows, abstract simplicial complexes are referred to as simplicial complexes.

**Definition 2.1** *Let  $\mathcal{X} = \{x_0, \dots, x_n\}$  be a finite set, and  $\Delta$  be a collection of non-empty subsets in  $\mathcal{X}$ . Then  $\Delta$  is said to be an abstract simplicial complex if it satisfies the following properties:*

1.  $\{x_i\} \in \Delta$  for all  $i = 0, \dots, n$ .
2. If  $\tau \in \Delta$  and  $\sigma \subseteq \tau$  such that  $\sigma \neq \emptyset$ , then  $\sigma \in \Delta$ .

The set  $\mathcal{X}$  is also called the vertex set of  $\Delta$  and the elements of  $\mathcal{X}$  are referred to as vertices. Note that an abstract simplicial complex is completely determined by its set of vertices. For an integer  $k \geq 0$ , any subset  $\sigma \in \Delta$  with  $k + 1$  vertices is said to be a  $k$ -simplex or a  $k$ -dimensional simplex. Any subset  $\tau$  of a  $k$ -simplex  $\sigma$  with  $k$  vertices is called a face of  $\sigma$ . The dimension of  $\Delta$  denoted as  $\dim(\Delta)$  is defined to be the maximum dimension of simplices in  $\Delta$ . That is,  $\dim(\Delta) \triangleq \max \{\dim(\sigma) : \sigma \in \Delta\}$ .

Now, we define the following algebraic structure on simplices in  $\Delta$  to define holes or cycles in different dimensions of a topological space. First, we need to assign orientations; an ordering on vertices of simplices in  $\Delta$ . Let  $\sigma = \{x_{i_0}, \dots, x_{i_k}\}$  be a  $k$ -simplex in  $\Delta$ , where  $i_0, \dots, i_k$  is a permutation of  $0, 1, \dots, k$ . We say two ordering of its vertex set is equivalent if they differ from one another by an even permutation. Thus, orderings of the vertices of  $\sigma$  fall into two equivalent classes. Each of these classes is referred to as an orientation of  $\sigma$ . A 0-simplex has only one orientation. For any  $k \geq 0$ , we denote an oriented simplex as  $[\sigma] = [x_{i_0}, \dots, x_{i_k}]$ .

We denote the set of all  $k$ -simplices in  $\Delta$  as  $\Delta_k$ . A  $k$ -chain on  $\Delta$  is defined to be a formal linear combination of  $k$ -simplices in  $\Delta_k$ . Let  $n_k = |\Delta_k|$ , and  $\gamma$  denotes a  $k$ -chain on  $\Delta$ , that is  $\gamma \triangleq \sum_{i=1}^{n_k} \alpha_i \sigma_i$ , where the coefficients  $\alpha_i$ 's belong to some field  $\mathbb{F}$ . The space of  $k$ -chains is a

vector space over the field  $\mathbb{F}$ , and defined as

$$C_k(\mathcal{X}, \mathbb{F}) \triangleq \left\{ \gamma = \sum_{i=1}^{n_k} \alpha_i \sigma_i : \alpha_i \in \mathbb{F} \right\}.$$

Now, we need to map the simplices in  $\Delta_k$  into a basis of  $C_k(\mathcal{X}, \mathbb{F})$  such that the map preserves orientations of simplices in  $\Delta_k$ . Let  $\Delta_k^\pi$  denote the set containing all the simplices in  $\Delta_k$  in all possible orientations. Any oriented simplex  $[\sigma]$  in  $\Delta_k^\pi$  is denoted as  $[x_{\pi(0)}, \dots, x_{\pi(k)}]$ , where  $\pi = \{\pi(0), \dots, \pi(k)\}$  is a permutation of  $0, \dots, k$ . Then, for any simplex  $\sigma_i \in \Delta_k$ , define the map  $T_k : \Delta_k^\pi \rightarrow C_k(\mathcal{X}, \mathbb{F})$  as follows:

$$T_k([x_{\pi(0)}^i, \dots, x_{\pi(k)}^i]) = (-1)^{P(\pi)} \mathbf{e}_i,$$

where  $P(\pi)$  is the parity of the permutation  $\pi$  and  $\mathbf{e}_i$  is the standard basis in  $\mathbb{R}^{n_k}$ .

A linear transformation  $\partial_k : C_k(\mathcal{X}, \mathbb{F}) \rightarrow C_{k-1}(\mathcal{X}, \mathbb{F})$  is called the boundary operator. The  $k^{\text{th}}$  boundary operator is a  $n_{k-1} \times n_k$  matrix  $\partial_k$  whose  $i^{\text{th}}$  column  $(\partial_k)_i$  is defined as follows:

$$(\partial_k)_i = \sum_{\sigma \in \Delta_{k-1}} T_{k-1}(\sigma),$$

where  $\sigma$  is face of  $\sigma_i$ . The subspaces  $B_k(\Delta) \triangleq \text{Im } \partial_{k+1}$  and  $Z_k(\Delta) \triangleq \ker \partial_k$  are the set of  $k$ -boundaries and the set of  $k$ -cycles, respectively. The  $k^{\text{th}}$  homology of  $\Delta$  is defined to be the quotient vector space given by

$$H_k(\Delta) \triangleq \ker \partial_k / \text{Im } \partial_{k+1}.$$

One of the refined topological invariants that are derived from the homology groups is Betti numbers. Betti numbers provide a quantitative description of topological features in a space. For any integer  $k \geq 0$ , we define the  $k^{\text{th}}$  Betti number,  $\beta_k$ , of  $\Delta$  as  $\beta_k \triangleq \dim (H_k(\Delta))$ . Betti numbers are important topological invariants that count the number of connected components and holes in a topological space. In particular,  $0^{\text{th}}$  Betti numbers count the number of connected components, and  $1^{\text{st}}$  order Betti numbers count the number of one-dimensional loops or cycles.

In practice, homology computation of a topological space  $\mathcal{X}$  from the finite set of observations  $\mathcal{X}_n = \{x_1, \dots, x_n\}$  from it, involves converting the data  $\mathcal{X}_n$  into simplicial complexes.

Simplicial complexes are constructed by identifying simplices of different dimensions, which requires defining the proximity of data points at some threshold, say  $r \geq 0$ . The proximity of data points at a threshold  $r$  is defined using some metric (say, Euclidean metric when data is embedded into an Euclidean space). The two frequently used constructions of simplicial complexes are the Čech complex and the Vietoris–Rips complex (see, e.g., [25]).

The choice of proximity threshold  $r$  is unknown in practice, and homology at a particular threshold is noisy. Therefore, one computes topological features (connected components and holes) at multiple thresholds and tracks the evolution of these features as thresholds vary. Then one considers a topological feature to be significant if it persists for a longer duration. This leads to the idea of persistent homology.

## 2.2 Persistent homology

Let  $\mathcal{X}$  be a space, then a filtration of  $\mathcal{X}$  is a nested family of spaces  $\{\mathcal{X}_t : t \in \mathbb{R}\}$  such that  $\mathcal{X} = \bigcup_{t \in \mathbb{R}} \mathcal{X}_t$ . There are two types of filtrations often used in TDA. First, filtrations built on top of a point cloud, for example, the families of Rips or Čech complex indexed over a set of non-negative real numbers. Second, filtrations obtained through level sets of a function  $f : \mathcal{X} \rightarrow \mathbb{R}$ , for example, one can take  $\mathcal{X}_t = \{x \in \mathcal{X} : f(x) \geq t\}$  to form a filtration of  $\mathcal{X}$ , such filtration is referred to as super-level set filtration of  $f$ . In practice, the index parameter  $t$  is called the scale parameter. The homology of the spaces  $\mathcal{X}_t$  varies with the scale parameter  $t$ . For example, as  $t$  increases, new connected components may be born, or existing connected components may disappear. Similarly, new holes or cycles are formed or filled up as  $t$  increases. Thus, as one moves through the filtration new features are born and existing features die. The birth time of a topological feature corresponds to the value of the scale parameter where it appears for the first time, and the death time of a feature corresponds to the value of the scale parameter where it dies or merges with another existing feature. Persistent homology tracks this process and records the pair of birth and death time of each topological feature in a multiset of points in  $\mathbb{R}^2$ , called persistence diagrams. One can refer to [21], [22], [37], [3] for rigorous treatment of persistent homology.

Given a filtration  $\{\mathcal{X}_t\}_{t \in \mathbb{R}}$  of a topological space  $\mathcal{X}$ , let, for any integer  $k \geq 0$ ,  $PH_k(\mathcal{X})$  denote the persistent homology of  $\mathcal{X}$  that tracks the evolution of  $k$ -dimensional topological features as the scale parameter varies. Let  $dgm_k$  denote the  $k^{th}$  persistence diagram; a multiset that consists of pairs of the birth and death time of  $k$ -dimensional topological features in  $PH_k(\mathcal{X})$ . Let  $(b, d)$  correspond to the birth and death pair of a feature in  $PH_k(\mathcal{X})$ , then the persistence of the feature is defined as  $d - b$ . Features that have higher persistence are generally considered significant features, and those that correspond to lower persistence are regarded as topological noise. Another equivalent and useful representation of features is via persistence barcodes (see [12], [25]). The persistence barcode is a set of intervals where endpoints correspond to the birth and death times of a feature. A bar in the persistence barcode is the length of the interval  $[b, d]$ . Individual bars corresponding to each feature are stacked on top of each other so that the resulting structure resembles a barcode.

Figure 1 depicts the persistent homology of the super-level set of a function via the persistence diagram and the persistence barcode. The leftmost figure is the graph of a non-negative function with three modes. We consider the super-level set filtration of the function to study the structures via the persistent homology. Note that at the level  $t > 0.20$ , the super-level set of the function is empty, hence there are no non-trivial connected components or cycles to study in this case. For  $t \leq 0$ , the super-level set of the function equals the entire domain  $[-10, 10]$ , implying that there is only one connected component in the super-level set. The interesting and non-trivial topological features occur when  $t \in (0, 0.20]$ . Note that at  $t = 0.20$ , the super-level set is  $\{0\}$  indicating the birth of a connected component. As we decrease  $t$ , new elements are added to the super-level set resulting in the birth and death of topological features. The green dotted lines indicate the levels at which a new connected component is born while the black dotted lines indicate the levels at which a connected component gets merged with the existing connected components. This process of evolution of features is summarized in the persistence diagram and the persistence barcode. Let  $[d, b]$  denote an interval in the persistence barcode then  $b$  corresponds to the birth of a topological feature and  $d$  corresponds to the death of a topological feature for a super-level set filtration. For the super-level set filtration, the birth of a connected component corresponds to a local maximum, and the death of a connected

component corresponds to a local minimum of the function.

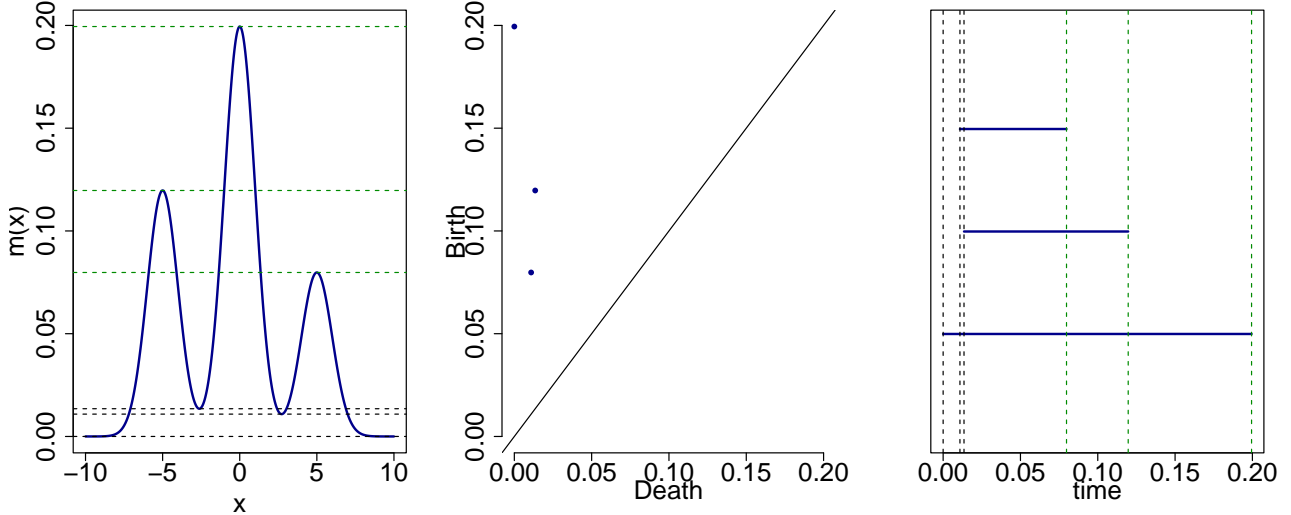


Figure 1: The graph of a function  $m$  (left). The persistence diagram of the super-level set filtration of  $m$  (middle). The persistence barcodes of  $m$  (right). The right endpoints of the bars in the barcode correspond to the local maxima, and the left endpoints correspond to the local minima of  $m$ . Green dotted lines indicate local maxima, and the black dotted lines indicate local minima.

In this article, we are mainly concerned with the persistent homology of the super-level set filtrations of a real-valued function  $f$ , which is unknown. Therefore, one observes finitely many values of  $f$  and estimates the persistent homology using an estimate  $\hat{f}$  of  $f$  (see, e.g., [23], [8], [9], [2], [10], [34]). The consistency of these procedures can be established using the well-known stability theorem for persistence diagrams (see [11]). We need to define the following terminology before giving the formal statement of the stability theorem.

**Definition 2.2 (Morse function)** *Let  $\mathcal{M}$  be a  $d$ -dimensional manifold, and  $f : \mathcal{M} \rightarrow \mathbb{R}$  be a twice differentiable function. A point  $p \in \mathcal{M}$  is said to be a critical point of  $f$  if  $\nabla f(p) = 0$ , and the value  $f(p)$  is called a critical value of  $f$ . A critical point  $p$  is said to be non-degenerate if the Hessian matrix evaluated at  $p$ , is non-singular. Then the function  $f$  is called a Morse function if all its critical points are non-degenerate, and all its critical values are distinct.*

**Definition 2.3 (Tame function)** Let  $\mathcal{M}$  be a  $d$ -dimensional manifold,  $f : \mathcal{M} \rightarrow \mathbb{R}$  be a continuous function, and for any  $t \in \mathbb{R}$ , define a super level set  $D_t = \{x \in \mathcal{M} : f(x) \geq t\}$ . Then, we say that  $t$  is a homological regular value if there exists  $\epsilon > 0$  such that for every  $a \leq b$  in  $(t - \epsilon, t + \epsilon)$  the map  $H_k(D_b) \rightarrow H_k(D_a)$ , induced by the inclusion of super level sets, is an isomorphism for every  $k \geq 0$ . Otherwise, we say that  $t$  is a homological critical value. Then the function  $f$  is said to be tame if it has finitely many homological critical values, and  $\dim(H_k(D_t)) < \infty$  for all  $t$  and  $k$ . Note that any Morse function on a compact manifold is tame.

**Definition 2.4 (Triangulable space)** Given a simplicial complex  $K$ , the underlying space is the union of the simplices of  $K$ . The underlying space of  $K$ , when viewed as a subset of an Euclidean space, is called a polytope. We say a topological space  $X$  is triangulable if there exists a finite simplicial complex with its polytope homeomorphic to  $X$ .

**Definition 2.5 (Bottleneck distance)** Let, for  $k \geq 0$ ,  $PH_k(f)$  and  $PH_k(g)$  denote the  $k$ -th persistent homology of the super-level set filtrations constructed via the continuous real-valued functions  $f$ , and  $g$ , respectively. Further, let  $dgm_k(f)$  and  $dgm_k(g)$  denote the  $k$ -th persistence diagrams corresponding to  $PH_k(f)$  and  $PH_k(g)$ , respectively. Then, the bottleneck distance between  $PH_k(f)$  and  $PH_k(g)$  is defined as:

$$\delta_B(PH_k(f), PH_k(g)) = \inf_{\gamma \in \Gamma} \sup_{p \in dgm_k(f)} \|p - \gamma(p)\|_\infty,$$

where the set  $\Gamma$  consists of all the bijections  $\gamma : dgm_k(f) \cup \text{diag} \rightarrow dgm_k(g) \cup \text{diag}$ , where  $\text{diag} = \{(b, d) : b = d\}$ , and  $\|\cdot\|_\infty$  denotes the sup-norm in  $\mathbb{R}^2$ .

Note that the cardinality of both persistence diagrams may differ. Therefore, to define bijections between two persistence diagrams, we add the diagonal line (diag) to each persistence diagram, where each point has infinite multiplicity. The features with longer lifetimes (persistence) are far from the diagonal line, while features with shorter lifetimes lie near the diagonal line. The bottleneck distance between two persistence diagrams can be considered a measure of the maximum amount of displacement required to make two diagrams identical. Now, we provide the formal statement of the stability theorem.

**Theorem 2.1 (Stability theorem) [11]** *Let  $f$  and  $g$  be real-valued continuous tame functions defined over the same triangulable space, and for any integer  $k \geq 0$ ,  $PH_k(f)$  and  $PH_k(g)$  denote the corresponding  $k^{\text{th}}$  persistent homology of  $f$  and  $g$ , respectively. Then we have,*

$$\delta_B (PH_k(f), PH_k(g)) \leq \|f - g\|_\infty.$$

### 3 Problem formulation and main results

Let  $(X_1, Y_1), \dots, (X_n, Y_n)$  be  $n$  independent replications of a bivariate random vector  $(X, Y)$ . Further, let  $F$  denote the joint distribution of  $(X, Y)$  with the joint probability density function  $f$ , and  $p$  denote the marginal density of  $X$ . Consider the following non-parametric regression model:

$$Y_i = m(x_i) + u_i, i = 1, \dots, n, \tag{3.1}$$

where  $x_i$ 's are observed values of the random variables  $X_i$ 's,  $u_i$ 's are unobserved errors assumed to be independent and identically distributed random variables with  $\mathbb{E}(u_i) = 0$  and  $var(u_i) = \sigma^2 (< \infty)$ , and  $m$  is the nonparametric regression function defined as  $m(x) \triangleq \mathbb{E}(Y|X = x)$ .

We aim to infer the geometric properties of the regression function  $m$  using its first-order derivative. Let  $m_1$  denote the first order derivative of the regression function  $m$ , we wish to summarize geometric features of  $m$  through the super-level sets of  $m_1$  which are defined as,

$$D_t = \{x \in \mathbb{R} : m_1(x) \geq t\}, t \in \mathbb{R}. \tag{3.2}$$

Note that  $\{D_t\}_{t \in \mathbb{R}}$  is a nested family of super-level sets as  $t$  decreases from  $\infty$  to  $-\infty$  that is for any  $t_1 < t_2$ , we have  $D_{t_2} \subset D_{t_1}$ . We use persistent homology for the filtration  $\{D_t\}_{t \in \mathbb{R}}$  to summarize the geometric features of  $m_1$ . Also note that  $m_1$  is unknown since  $m$  is unknown, so we estimate persistent homology of  $m_1$  from the observed data  $\mathcal{X}_n \triangleq \{(X_1, Y_1), \dots, (X_n, Y_n)\}$ . The common procedure is to use an estimate  $\hat{f}$  to estimate the persistent homology of an unknown function  $f$ .

However, as mentioned previously, due to the uncertainty of stability results, we resort to the procedure developed in [1]. The main results in [1] present a robust estimator of homology

for the level sets of density and regression functions. Then using this robust estimator of homology, the procedure for computing persistent homology is extended. We need the following definition before defining the procedure formally.

**Definition 3.1** *Let  $t \in \mathbb{R}$  be a level of  $D_t$  (see, Equation 3.2), and  $\epsilon \in (0, |t|/2)$ . We say that  $t$  is  $\epsilon$ -regular if the following holds:*

$$\begin{aligned} \partial D_{t+2\epsilon} \cap \partial D_{t+(3/2)\epsilon} &= \partial D_{t+(1/2)\epsilon} \cap \partial D_t = \partial D_t \cap \partial D_{t-(1/2)\epsilon} \\ &= \partial D_{t-(3/2)\epsilon} \cap \partial D_{t-2\epsilon} = \emptyset, \end{aligned}$$

where  $\partial A$  denotes the boundary of the set  $A$  and  $\emptyset$  denotes the empty set. In particular, if the underlying function  $f$  is continuous on  $f^{-1}[t - 2\epsilon, t + 2\epsilon]$ , then  $t$  is  $\epsilon$ -regular.

The procedure proposed by [1] is summarized as follows:

1. Let  $f : \mathbb{R}^d \rightarrow \mathbb{R}$  be a continuous tame (see, Definition 2.3) and bounded function. In this paper  $f = m_1$  and  $d = 1$ . Consider a super-level set  $D_t$  of  $f$ , and assume that the level  $t$  is  $\epsilon$ -regular (see, Definition 3.1).
2. Using the data  $(X_1, Y_1), \dots, (X_n, Y_n)$  construct an estimator  $\hat{f}_n$  using a kernel function  $K$  with the bandwidth  $h \equiv h(n)$ , and define

$$\mathcal{X}_n^t \triangleq \{X_i : \hat{f}_n(X_i) \geq t, i = 1, \dots, n\}. \quad (3.3)$$

3. Now use  $\mathcal{X}_n^t$  to construct an estimator of the super-level set  $D_t$  as

$$\hat{D}_t(n, h) \triangleq \bigcup_{x \in \mathcal{X}_n^t} \mathbb{B}_h(x), \quad (3.4)$$

where  $h \equiv h(n)$  is the kernel bandwidth, and  $\mathbb{B}_h(x)$  denotes a ball of radius  $h$  centered around the point  $x$ .

4. Note that for any  $\epsilon \in (0, |t|)$ , we have  $\hat{D}_{t+\epsilon}(n, h) \subset \hat{D}_{t-\epsilon}(n, h)$ . This gives an inclusion map from  $\hat{D}_{t+\epsilon}(n, h)$  to  $\hat{D}_{t-\epsilon}(n, h)$ .

5. The inclusion map  $i : \hat{D}_{t+\epsilon}(n, h) \hookrightarrow \hat{D}_{t-\epsilon}(n, h)$  induces a map in homology

$$i_k : H_k(\hat{D}_{t+\epsilon}(n, h)) \rightarrow H_k(\hat{D}_{t-\epsilon}(n, h)),$$

where  $k$  is any arbitrary degree of homology, and  $h \equiv h(n)$  is the kernel bandwidth.

6. Now, use the image of the map  $i_k$  as the robust estimator of homology denoted as  $\hat{H}_k(t, \epsilon; n)$ . Thus, for any arbitrary degree of homology  $k$ , we have

$$\hat{H}_k(t, \epsilon; n) \triangleq \text{Im}(i_k). \quad (3.5)$$

7. Define the following:

$$N_\epsilon \triangleq \sup_{x \in \mathbb{R}^d} \lceil f(x)/2\epsilon \rceil, t_{max} = 2\epsilon N_\epsilon \text{ and } t_i = t_{max} - 2i\epsilon, i \in \mathbb{Z}, \quad (3.6)$$

where  $\lceil x \rceil$  denotes the smallest integer larger than or equal to  $x$ .

8. Now, estimate the homology using  $\hat{H}_k(t_i, \epsilon; n)$  for every  $i \in \mathbb{Z}$ , and compute the persistent homology for the following discrete filtration  $\hat{\mathcal{D}}^\epsilon \triangleq \{\hat{D}_{t_i}(n, h)\}_{i \in \mathbb{Z}}$ . We denote this estimator of persistent homology as  $\widehat{PH}_k^\epsilon(f)$ .

In this paper, we establish the consistency of  $\widehat{PH}_k^\epsilon(f)$  when  $f = m_1$ . We estimate  $m_1$  using the Nadaraya-Watson estimator (see [35]) of the regression function  $m$ . That is, first, we estimate  $m$  as

$$\hat{m}_n(x) = \frac{\sum_{i=1}^n K_h(x - X_i) Y_i}{\sum_{i=1}^n K_h(x - X_i)}, \quad (3.7)$$

where  $K$  is a kernel function,  $h \equiv h(n)$  is kernel bandwidth and  $K_h(x) = K(x/h)$ . We require point-wise consistency of  $\hat{m}_n(x)$  for theoretical considerations in this paper. Therefore, we assume the following regularity conditions on the Kernel function:

(A.1) The kernel function  $K$  is a proper probability density function.

(A.2) The support of kernel  $K$  is a set  $S \subseteq [-1, 1]$  such that  $K(x) = K(-x)$  for all  $x \in S$ .

(A.3)  $K(x) \in [0, 1] \forall x \in S$  such that  $K(0) = 1$ .

(A.4) The kernel function  $K$  is bounded away from 0, that is  $\inf_{x \in S} K(x) = \delta$  where  $\delta > 0$ .

Then under the Assumptions (A.1) - (A.4), Theorem 2.1 of [31] states that if  $x \in \mathbb{R}$  with  $p(x) \neq 0$  is a continuous point of  $p$  (marginal density of  $X$ ),  $m$  (the regression function), and  $f$  (joint density of  $(X, Y)$ ) for each fixed  $y \in \mathbb{R}$ , then

$$\hat{m}_n(x) \xrightarrow{a.s.} m(x) \text{ as } h \rightarrow 0 \text{ and } n \rightarrow \infty \text{ such that } nh \rightarrow \infty. \quad (3.8)$$

Now, we define the estimator of  $m_1(x)$  as the first order derivative of  $\hat{m}_n(x)$ , that is

$$\hat{m}_{1,n}(x) = \frac{d}{dx} \hat{m}_n(x) = \frac{\sum_{i=1}^n Y_i K_{1,h}(x - X_i)}{\sum_{i=1}^n K_h(x - X_i)} - \frac{\sum_{i=1}^n Y_i K_h(x - X_i) \sum_{i=1}^n K_{1,h}(x - X_i)}{\left( \sum_{i=1}^n K_h(x - X_i) \right)^2}, \quad (3.9)$$

where  $K_{1,h}(x - X_i) = \frac{d}{dx} K_h(x - X_i)$  assuming that first order derivative of the kernel function  $K$  exists. In addition, we assume the following conditions on the first order derivative of  $K$  denoted as  $K_1$ :

(A.5) For any real number  $\tau > 0$  we have  $|K_1(x)| \leq \tau$  for all  $x \in S$  and  $K_1(0) = 0$ .

We need the following assumptions on the response variables, regressors, the regression function  $m$ , and its derivative  $m_1$  to establish the consistency of  $\widehat{PH}_k^\epsilon(m_1)$ .

(B.1) The marginal density of  $X$  denoted as  $p$  is tame (see, Definition 2.3) and bounded.

(B.2) The support of  $p$  is a compact set  $\mathcal{X}$ , and  $p_{min} = \inf_{x \in \mathcal{X}} p(x) > 0$ , and  $p_{max} = \sup_{x \in \mathcal{X}} p(x)$ .

(B.3) The response variable satisfies  $|Y| \leq Y_{max}$  almost surely,  $Y_{max}$  is a positive real number.

(B.4) The regression function  $m$  is continuous, and  $|m(x)| \leq M$  for all  $x \in \mathbb{R}$ , where  $M > 0$ .

(B.5) The derivative of the regression function  $m_1$  is tame and continuous on a compact domain, and  $|m_1(x)| \leq M_1$  for all  $x \in \mathbb{R}$ , where  $M_1$  is a positive constant.

Now, we state the main result of the consistency of  $\widehat{PH}_k^\epsilon(m_1)$  in the following theorem.

**Theorem 3.1** *If  $h \equiv h(n) \rightarrow 0$  as  $n \rightarrow \infty$  such that  $nh^2 \rightarrow \infty$ , then under the Assumptions (A.1) - (A.5) and (B.1) - (B.5), we have*

$$\mathbb{P} \left( \delta_B \left( \widehat{PH}_k^\epsilon(m_1), PH_k(m_1) \right) \leq 5\epsilon \right) \geq 1 - 3N_\epsilon n e^{-C_{\epsilon/2} n h^2},$$

where  $k$  is any arbitrary degree of homology,  $\delta_B$  is the bottleneck distance (see, Definition 2.5),  $N_\epsilon$  is defined in Equation 3.6, and

$$C_\epsilon = \frac{2\epsilon^2\delta^2 p_{min}^2}{[\tau(Y_{max} + M) + (M_1 + \epsilon)]^2}.$$

Here  $M$ ,  $M_1$ ,  $Y_{max}$ ,  $\tau$ ,  $\delta$  and  $p_{min}$  are the same as defined in (B.4), (B.5), (B.3), (B.2), (A.4) and (A.5), respectively.

**Remark 3.1** Note that, the constant  $C_\epsilon$  must be positive in order to have a valid lower bound of the probability in Theorem 3.1. Since if  $C_\epsilon = 0$ , then the sequence  $1 - 3N_\epsilon n e^{-C_\epsilon/2nh^2} = 1 - 3N_\epsilon n < 0$ . Furthermore, as  $n \rightarrow \infty$  the sequence goes to  $-\infty$  implying that the proposed procedure is not consistent. For this reason, we need to assume that  $\delta > 0$  as precisely defined in Assumption (A.4).

Theorem 3.1 states that the estimator  $\widehat{PH}_k^\epsilon(m_1)$  is consistent up to the precision of  $5\epsilon$ . However, one can choose  $\epsilon$  arbitrarily small to acquire higher precision. Note that  $\epsilon \in (0, |t|/2)$  such that the condition in Definition 3.1 is satisfied. We have assumed that the levels are  $\epsilon$ -regular (see, Definition 3.1). Therefore, such an  $\epsilon$  always exists, and we need not choose the precise value of  $\epsilon$ , instead choosing any lower bound will suffice. Note that the smaller the value of  $\epsilon$ , the smaller the value of  $C_\epsilon$  will be, and the convergence of  $\widehat{PH}_k^\epsilon(m_1)$  to  $PH_k(m_1)$  will be slower.

The sketch of the proof is as follows. Let  $\mathcal{D}$  denote the continuous filtration and  $\mathcal{D}^\epsilon$  denote the discrete version of  $\mathcal{D}$  with step size  $2\epsilon$ . In the present context, we estimate the persistent homology corresponding to the filtration  $\mathcal{D}^\epsilon$ . Therefore, the maximum difference between the persistent homology of  $\mathcal{D}$  and  $\mathcal{D}^\epsilon$  is  $2\epsilon$ . Hence, to prove Theorem 3.1 it is enough to show that the maximum difference between estimated persistent homology and true persistent homology of  $\mathcal{D}^\epsilon$  is  $3\epsilon$ . As pointed out in [1], this can be done using the language of  $\epsilon$ -interleaving introduced in [7]. Thus, using the weak stability theorem from [7], and Lemma 8.2, proof of Theorem 3.1 is established.

## 4 Statistical significance of local structures

In the following sections, we apply Theorem 3.1 in identifying the local structures such as monotonicity, convexity, and modality in smooth regression curves. One major challenge in inferring local structures of regression functions from a finite data set is assessing their statistical significance. A quantitative statistical assessment is important to determine whether the observed local structures are signals or artifacts of sampling noise. In the present context, local structures are derived from the 0-dimensional estimated persistence barcodes computed using the procedure given in Section 3 whose validity is guaranteed by Theorem 3.1. Therefore, we translate the statistical significance of the observed local structures in terms of the statistical significance of the 0-dimensional topological features (connected components) in the estimated barcode.

There are various procedures to assess the statistical significance of topological features in estimated barcodes obtained from continuous filtrations by existing procedures (see, e.g., [23]). However, in the present context, we compute barcodes from a discrete filtration using the method proposed by [1] that does not have similar results as in the case of continuous filtration. The main reason is that most existing procedures for examining the statistical significance require stability results for persistence barcodes. In contrast, we do not have the stability results for persistence barcodes in the present context.

We propose a measure of statistical significance of the observed 0-dimensional topological features in the estimated barcodes calculated from the procedure described in Section 3. We translate the statistical significance of the 0-dimensional topological features in the estimated barcodes in terms of the statistical significance of the critical values of the estimated derivative. Since for the super level-set filtrations of the Morse and tame functions, topological features in the 0-dimensional persistence barcodes are born and die at the critical values of the functions. Also, note that, for any  $k \geq 0$ , the birth and the death time of a  $k$ -dimensional topological feature completely characterize the topological feature in the  $k$ -dimensional barcode. Consequently, it is equivalent to having the statistical significance of the birth and the death times of topological features in the barcode to have the statistical significance of the topological features

in the estimated barcode. Hence, we measure the statistical significance of the critical values of the estimated derivative to measure the statistical significance of the 0-dimensional topological features in the estimated barcode. To do this, let us simplify the expression of the estimated derivative given in Equation (3.9), We have

$$\hat{m}_{1,n}(x) = \frac{\sum_{i=1}^n K_{1,h}(x - X_i) (Y_i - \hat{m}_n(x))}{\sum_{i=1}^n K_h(x - X_i)} = \sum_{i=1}^n \omega_i(x) r_i(x), \quad (4.1)$$

where  $\omega_i(x) = \frac{K_{1,h}(x - X_i)}{\sum_{i=1}^n K_h(x - X_i)}$  are weights to the  $i$ -th residual  $r_i(x) = Y_i - \hat{m}_n(x)$ ,  $i = 1, \dots, n$ .

Note that, from Equation (4.1), for any fix  $x_0 \in \mathbb{R}$ , the value  $\hat{m}_{1,n}(x_0)$  is the weighted sum of the residuals  $r_i(x_0)$ ,  $i = 1, \dots, n$ . Given this fact, we declare  $\hat{m}_{1,n}(x_0)$  to be significantly different from noise (statistically significant) if the residuals  $r_i(x_0)$  that have larger values contribute less in Equation 4.1 compared to those that have smaller values. In other words, we declare the value  $\hat{m}_{1,n}(x_0)$  to be statistically significant if the larger weights are assigned in the corresponding Equation 4.1 to the residuals that have smaller values. In particular, if we observe a significantly decreasing trend between the residuals  $r_i(x_0)$ , and the weights  $\omega_i(x_0)$  for all  $i = 1, \dots, n$ , we say that the value  $\hat{m}_{1,n}(x_0)$  is statistically significant. This phenomenon can be captured by fitting a linear regression model with  $r_i(x_0)$  as the response variable and  $\omega_i(x_0)$  as a regressor, for  $i = 1, \dots, n$ . Consider the following linear regression model:

$$r_i(x_0) = \beta_0 + \beta_1 \omega_i(x_0) + \eta_i, i = 1, \dots, n \quad (4.2)$$

where  $\beta_0$  and  $\beta_1$  are unknown parameters and  $\eta_i$  is unobserved random error in the model with the usual error assumptions. We say that the value  $\hat{m}_{1,n}(x_0)$  is statistically significant if the estimate of  $\beta_1$  is negative and statistically significant.

Now, we illustrate the procedure described above. Suppose that we observe a barcode with  $p$  0-dimensional topological features, say  $\mathcal{B}_0 = \{[a_1, b_1], \dots, [a_p, b_p]\}$ ,  $p$  is a finite positive integer, from the super-level set filtration of the estimated derivative  $\hat{m}_{1,n}$  using the procedure described in Section 3. Then for each 0-dimensional feature  $[a_i, b_i]$  in  $\mathcal{B}_0$ , there exists critical points,  $x_i^a, x_i^b \in \mathbb{R}$ , of  $\hat{m}_{1,n}$  such that  $\hat{m}_{1,n}(x_i^a) = a_i$ , and  $\hat{m}_{1,n}(x_i^b) = b_i$ , respectively, for  $i = 1, \dots, p$ .

We say that a feature  $[a_i, b_i]$  in  $\mathcal{B}_0$  is statistically significant if both the values  $\hat{m}_{1,n}(x_i^a) = a_i$ , and  $\hat{m}_{1,n}(x_i^b) = b_i$  are statistically significant; otherwise, we say that the feature is statistically insignificant, for  $i = 1, \dots, p$ . We demonstrate this procedure on simulated and real data in the following sections.

## 5 Simulation studies

This section presents some applications of Theorem 3.1 to infer the monotonicity, convexity, and modality of smooth regression curves underlying the data. We simulate noisy observations from smooth regression curves and characterize the aforementioned local structures using the methodology proposed in Section 4. We infer local structures of the underlying regression curves over a grid of points in the region  $[-1, 1]$ .

In addition, we compare the results with a graphical device called SiZer map, an existing procedure for exploring structures such as peaks and valleys in smooth regression curves proposed by [6]. The SiZer map visualizes significant features such as bumps simultaneously over both location and scale (bandwidth) by using a color map. The idea is to highlight the regions in the location-scale space where the curve significantly increases and decreases. The idea is motivated by the fact that the significant bumps will be at *zero crossings of the derivative between regions of significant increase and decrease*. Hence, the name “SiZer” is given for “Significant ZERo crossings of derivatives”. The color scheme on the SiZer map is as follows: **Blue** is used to indicate regions where the curve is significantly increasing; **Red** is used to indicate regions where the curve is significantly decreasing; **Purple** is used to indicate regions where the curve cannot be concluded to be either significantly increasing or decreasing; **Gray** is used to indicate regions where there are not enough data points to make statements about the significance of the features. The dotted curves in SiZer maps show effective window widths for each bandwidth as intervals representing  $\pm 2h$ .

We provide a quantitative evaluation of local structures using the methodology proposed in Section 4, and compare the results with the respective SiZer maps. The statistical significance of the features in the estimated barcode is tabulated in the following manner. Let  $\mathcal{B} = \{[a_i, b_i] :$

$a_i < b_i, i = 1, \dots, p\}$  be an observed barcode with  $p$  0-dimensional features. Note that features in  $\mathcal{B}$  are ordered in increasing order of persistence (length of the intervals). We tabulate the estimated slope of the regression line defined in Equation (4.2), and its p-value, for each  $a_i, b_i \in \mathcal{B}$ . The estimated slope is denoted by  $\hat{\beta}_1$ . In addition, we tabulate the critical points, denoted by  $\hat{c}_p$ , corresponding to each  $a_i, b_i \in \mathcal{B}$  to compare the results with the SiZer maps. Recall that each  $a_i, b_i \in \mathcal{B}$  constitutes the set of critical values of the estimated regression function. This allows one to compare the observed structure inferred from the barcode with the respective SiZer maps. In particular, let  $[a, b], a < b$  be an observed 0-dimensional feature in the barcode of the estimated derivative, where  $a$  and  $b$  denote the death and birth times, respectively. Further, let  $a > 0$ , that is the observed death time is positive implying that  $\hat{m}$  is an increasing function. Now, visualize the critical point corresponding to the death time  $a$  on the SiZer map of  $\hat{m}$ . If the critical point lie on, say, blue region, indicating the  $\hat{m}$  is significantly increasing, then both the conclusions coincide. Otherwise, the inferences drawn from the SiZer maps and the proposed procedure based on the barcode of the estimated derivative are contrary.

In what follows, we provide simulation results for the normal and Cauchy kernel supported on  $[-1, 1]$ . However, we compare the results with the SiZer maps only for the Gaussian kernel since the conventional SiZer is applicable only for the Gaussian kernel.

## 5.1 Monotonicity

We characterize the monotonicity of a smooth and bounded regression function using the 0-dimensional features of the barcode of the first derivative. The main idea is that the birth and death time corresponding to the 0-dimensional feature with the largest persistence in a barcode provide the maximum and minimum value of the function, respectively (see, Figure 1). Therefore, we can extract the 0-dimensional feature with the largest persistence from the barcode of the first derivative to characterize the monotonicity of the function. In particular, if the death time of the feature is non-negative, that is the minimum value of the first derivative is non-negative, then the function is non-decreasing. Similarly, if the birth time of the feature is non-positive, that is the maximum value of the first derivative is non-positive, then the function

is non-increasing.

Consider the regression function  $m(x) = e^x, x \in [-1, 1]$  to investigate its monotonicity from kernel estimates of its derivative  $m_1$ . The kernel estimates of  $m$  and  $m_1$  are shown in Figure 2 where a Gaussian kernel truncated on  $[-1, 1]$  is used for the sample size  $n = 50$ , and for three different bandwidths  $h \in \{n^{-1/3}, n^{-1/5}, n^{-1/7}\}$ . The error distribution is the normal distribution truncated on  $[-1, 1]$  with mean 0 and variance 0.1. It is evident from Figure 2 that  $m$  is estimated well while its derivative  $m_1$  is not for each of the bandwidths. The monotonicity (non-decreasingness) of  $m$  is evident from the visual inspection of the estimates of  $m$ . However, a quantitative assessment, such as statistical hypothesis testing, is needed to ensure that the observed monotone structure is significant, and not an artifact of sampling noise.

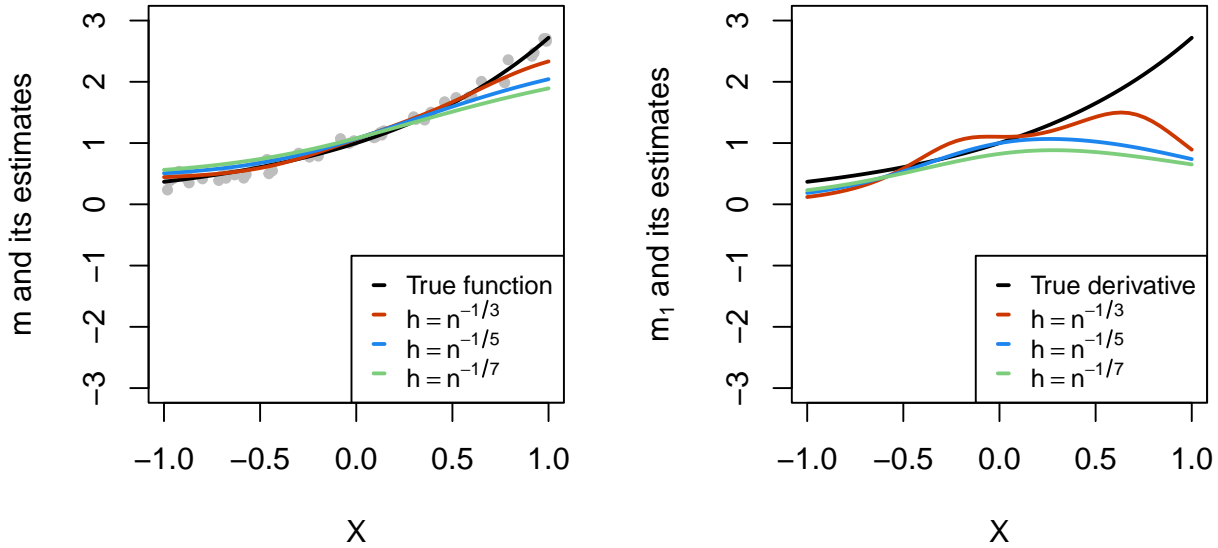


Figure 2: Estimates of  $m$  and  $m_1$  using a Gaussian kernel truncated on  $[-1, 1]$ .

We obtain barcodes for the estimated derivative,  $\hat{m}_1$ , using the procedure mentioned in Section 3, and use the proposed procedure articulated in Section 4 to infer the monotonicity of  $m$  from the observed data. The observed barcodes for different bandwidths are  $\{[0.1, 1.4]\}$ ,  $\{[0.1, 1]\}$ ,  $\{[0.2, 0.8]\}$  for the bandwidths  $h = n^{-1/3}, h = n^{-1/5}, h = n^{-1/7}$ , re-

spectively. These barcodes are obtained with the filtration parameters  $\epsilon = 0.1$  and the discrete grid of integers  $G = \{-g, -g+1, \dots, g-1, g\}$ , here  $g = 20$ . It is evident from the death times of the observed features in the barcode that the function underlying the observed data is strictly increasing for each of the three bandwidths. The true and estimated barcodes are depicted in Figure 3 where the gray dotted lines intersect the time axis at the death times of the features. Note that the time axis represents the values  $t_i, i \in G$ , where  $t_i$  is defined in Equation (3.6).

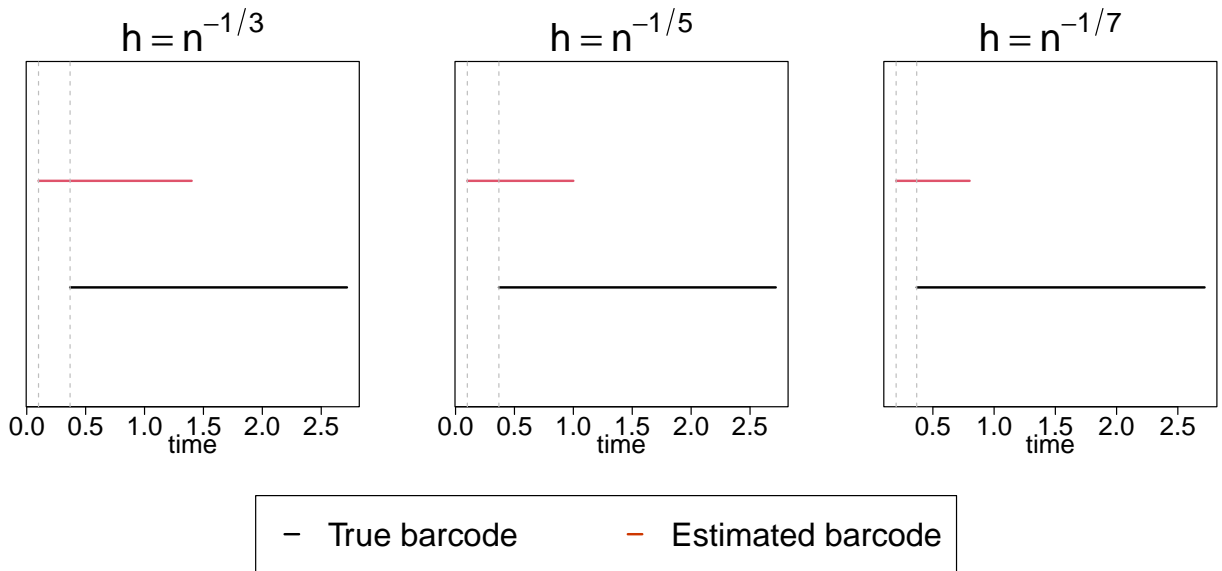


Figure 3: Estimated barcodes for  $n = 50$  for a Gaussian kernel truncated on  $[-1, 1]$ .

Next, we increase the sample size from  $n = 50$  to  $n = 100$  to further examine this observed monotone structure. The estimated barcodes for  $n = 100$  are  $\{[0.1, 1.8]\}$ ,  $\{[0.2, 1]\}$ ,  $\{[0.2, 0.8]\}$  for each of the three bandwidths, respectively. These barcodes are shown in Figure 4, suggesting that the estimated function is strictly increasing.

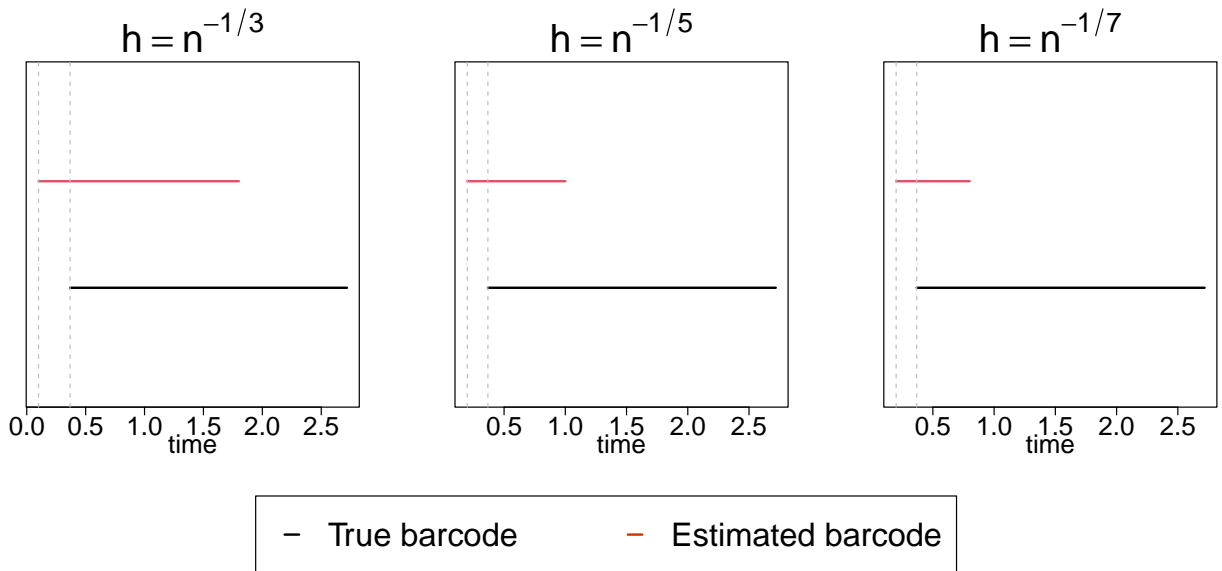


Figure 4: Estimated barcodes for  $n = 100$  for Gaussian kernel truncated on  $[-1, 1]$ .

We provide a quantitative assessment of this observed monotone structure using the procedure proposed in Section 4, and compare the results with the respective SiZer maps. It is evident from Table 1 that the observed death times ( $a_1$ ) for each of the bandwidths and sample sizes are significant. Since the corresponding  $\hat{\beta}_1$  (see, Equation (4.2)) is negative and significant. Moreover, the critical points ( $\hat{\mathbf{c}}_p$ ) corresponding to the death times of the observed features lie in the blue region on the SiZer map (see, Figure 5) implying that the observed structure is non-decreasing and significant at these points for each of the three bandwidths. This implies that the death times of the observed features are non-negative and significant, consistent with the results in Table 1. Note that green dots highlight the critical points, and the bandwidths  $h = n^{-1/3}, n^{-1/5}, n^{-1/7}$  are depicted through black, gray, and red dotted lines, respectively, on the SiZer map (see, Figure 5).

Table 1: Significance of Monotonicity for Gaussian Kernel.

	For $n = 50$			For $n = 100$		
	$h = n^{-1/3}$	$h = n^{-1/5}$	$h = n^{-1/7}$	$h = n^{-1/3}$	$h = n^{-1/5}$	$h = n^{-1/7}$
	$\mathbf{a}_1$	$\mathbf{a}_1$	$\mathbf{a}_1$	$\mathbf{a}_1$	$\mathbf{a}_1$	$\mathbf{a}_1$
$\hat{\mathbf{c}}_p$	-1	-1	-1	-1	-1	-1
$\hat{\beta}_1$	-7.5	-18.2	-26.2	-7.2	-23.5	-40.1
p-value	$< 10^{-8}$	$< 10^{-8}$	$< 10^{-7}$	$< 10^{-11}$	$< 10^{-16}$	$< 10^{-16}$

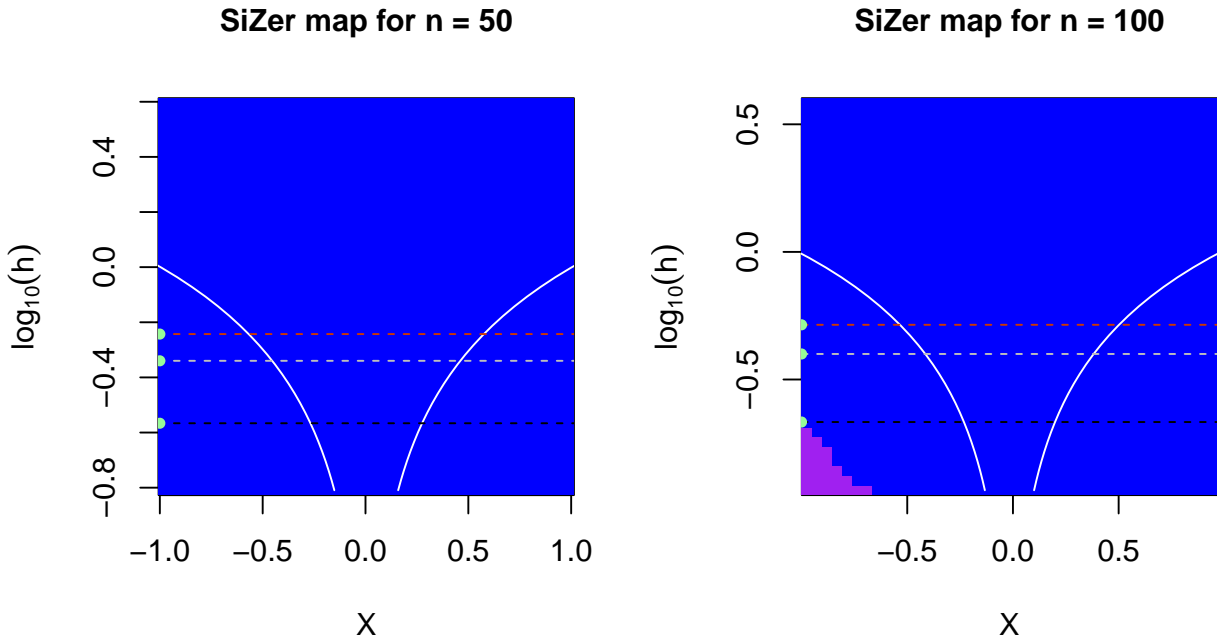


Figure 5: SiZer analysis of the regression function to investigate its monotonicity.

Next, we demonstrate kernel estimates of  $m$  and  $m_1$  for the Cauchy kernel truncated at  $[-1, 1]$  in Figure 6. It can be seen in Figure 6 that the estimates of  $m_1$  are too noisy for each of the bandwidths, while  $m$  is quite well estimated. To investigate the monotonicity of  $m$ , the estimated barcodes of the derivative are shown in Figure 7. The estimated barcodes for the bandwidths  $h \in \{n^{-1/3}, n^{-1/5}, n^{-1/7}\}$  are  $\{[-0.03, 1.24]\}$ ,  $\{[0.02, 0.84]\}$ ,  $\{[0.04, 0.73]\}$ ,

respectively. The monotonicity of the estimated  $m$  is not evident for  $h = n^{-1/3}$  as the death time in the barcode of the derivative is negative. Furthermore, the observed non-monotone structure is significant for  $h = n^{-1/3}$  as it can be seen in Table 2. On the other hand, for the bandwidths  $h = n^{-1/5}$  and  $h = n^{-1/7}$ , the observed structure of the estimated  $m$  is significantly non-decreasing. Since the death times in the observed barcodes are non-negative and significant from Table 2.

Now, we increase the sample size from  $n = 50$  to  $n = 100$  to further examine the monotonicity of  $m$ . The observed barcodes of the derivative for the three bandwidths are  $\{[-0.08, 1.50], [0, 0.94], [0.04, 0.75]\}$ . Again, it is evident that the observed structure is significantly non-monotone for  $h = n^{-1/3}$ , and significantly non-decreasing for  $h = n^{-1/5}$  and  $h = n^{-1/7}$ . The significance of the death times ( $a_1$ ) in the observed barcode of the derivative is articulated in Table 2 for different bandwidths and sample sizes.

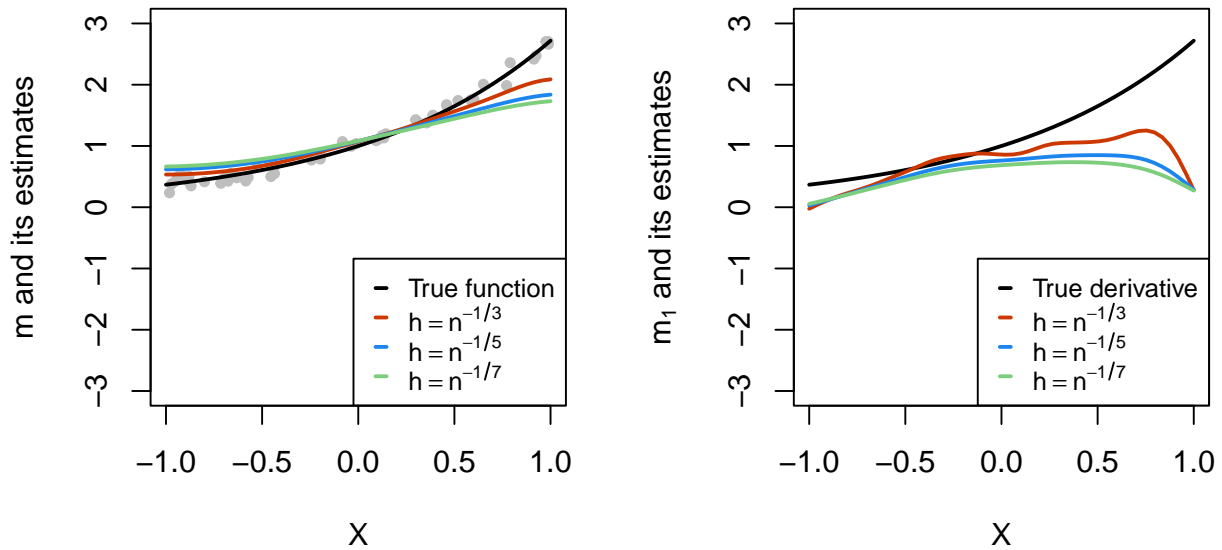


Figure 6: Kernel estimates using the Cauchy kernel truncated on  $[-1, 1]$ .

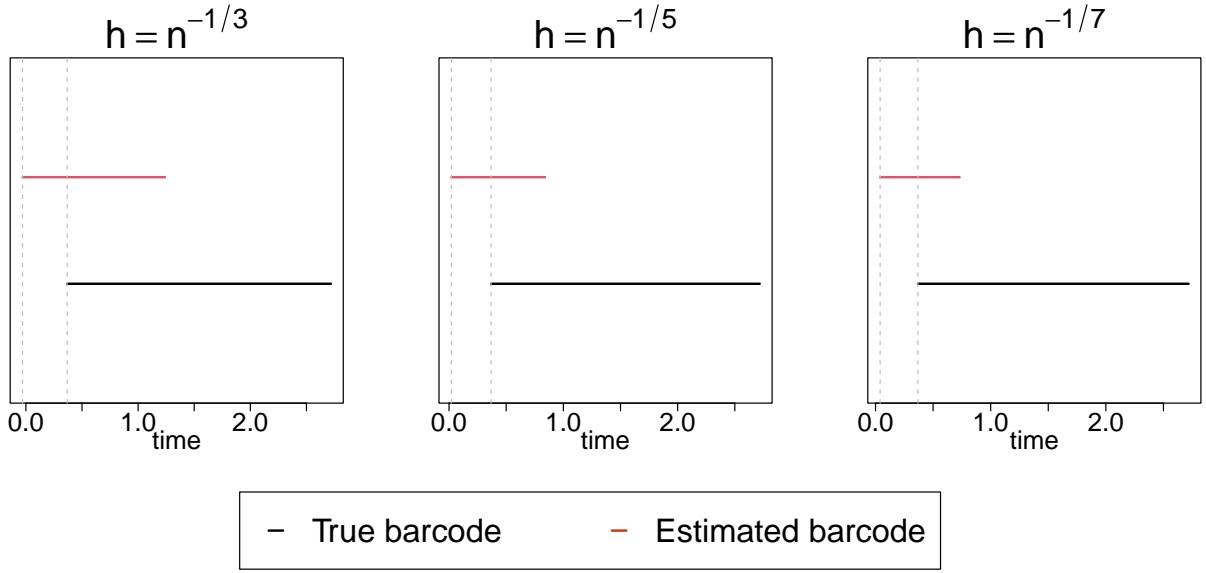


Figure 7: Estimated barcodes for  $n = 50$  the Cauchy kernel truncated on  $[-1, 1]$ .

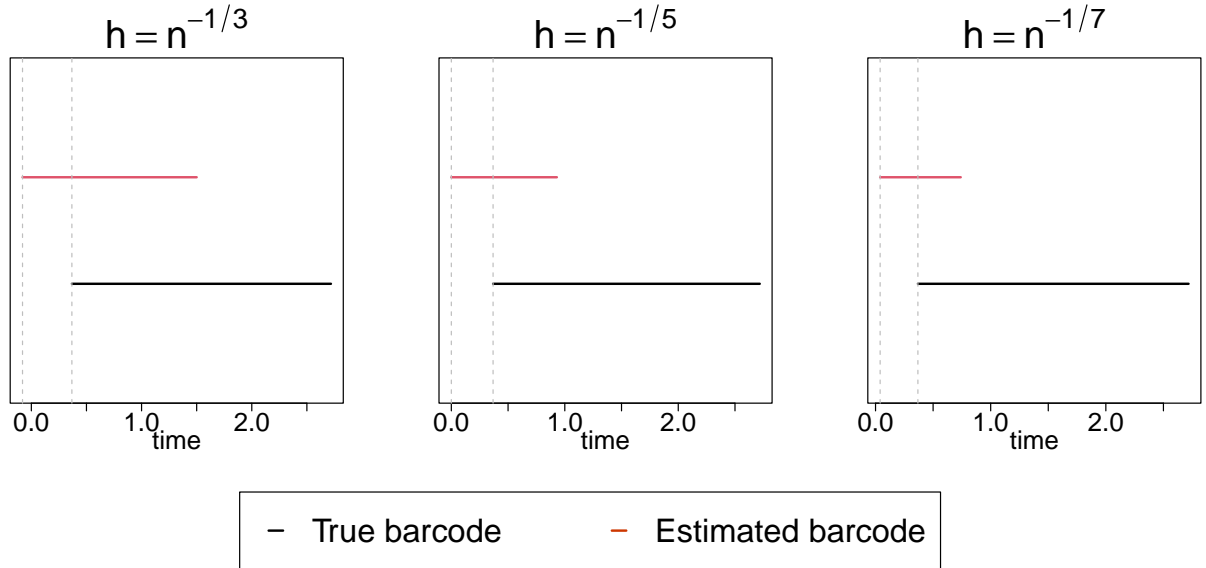


Figure 8: Estimated barcodes for  $n = 100$  Cauchy kernel truncated on  $[-1, 1]$ .

## 5.2 Convexity

We provide an illustrative example to infer the convexity of a smooth regression function from noisy samples using estimated barcodes of its first derivative. We characterize the convexity

Table 2: Significance of Monotonicity for Cauchy Kernel.

	For $n = 50$			For $n = 100$		
	$h = n^{-1/3}$	$h = n^{-1/5}$	$h = n^{-1/7}$	$h = n^{-1/3}$	$h = n^{-1/5}$	$h = n^{-1/7}$
	$\mathbf{a}_1$	$\mathbf{a}_1$	$\mathbf{a}_1$	$\mathbf{a}_1$	$\mathbf{a}_1$	$\mathbf{a}_1$
$\hat{\mathbf{c}}_p$	-1	-1	-1	-1	-1	-1
$\hat{\beta}_1$	-8.8	-21.6	-30.2	-8.8	-28.4	-45.7
<b>p-value</b>	$< 10^{-8}$	$< 10^{-10}$	$< 10^{-9}$	$< 10^{-11}$	$< 10^{-16}$	$< 10^{-16}$

(equivalently, concavity) of a function  $f$  on  $[-1, 1]$  by the fact that there exists a critical point of  $f$ , say,  $c \in [-1, 1]$  such that  $f$  is non-decreasing (non-increasing) in  $[c, 1]$  and non-increasing (non-decreasing) in  $[-1, c]$ . However, as one of the reviewers pointed out, this characterization is not valid for some functions. For instance, consider the function  $m(x) = \frac{x^2}{1 + x^2 + x|x|}$ ,  $x \in [-1, 1]$ . The reason is that the convexity of  $m$  requires its first derivative  $m_1$  to be non-decreasing in  $[-1, 1]$ , while the characterization captures only the monotone structure of  $m$  on  $[c, 1]$  and  $[-1, c]$  rather than the monotonicity of  $m_1$  on  $[-1, 1]$ . This suggests modifying the characterization to account for the monotone structure of  $m_1$  on  $[-1, 1]$  to infer the convexity of  $m$  on  $[-1, 1]$ .

Note that to characterize the monotone structure of  $m_1$  quantitatively, we need to consider the barcodes of the second derivative of  $m$ . However, qualitatively, the monotonicity of  $m_1$  can be captured by comparing the barcodes of  $m_1$  and  $-m_1$ , as also suggested by one of the reviewers. The rationale behind the argument is that for a monotone function  $f$ , the super-level set  $D_t = \{x : f(x) \geq t\}$  of  $f$  has only a single connected component, for every  $t \in \mathbb{R}$ . However, this is not a necessary condition since if  $f$  is a concave shape function, then also  $D_t$  will have only a single connected component for every  $t \in \mathbb{R}$  (see, Figure 19). Therefore, to rule out such situations we have to make use the property of monotone functions that if  $f$  is monotone increasing (decreasing) on an interval  $[a, b]$  (here we take  $a = -1$ ,  $b = 1$ ), then  $-f$  will be monotone decreasing (increasing) on  $[a, b]$ . This property allows us to characterize the monotonicity of a function  $f$  from the barcodes of  $f$  and  $-f$ . Note that in Section 5.1, we characterize the monotonicity quantitatively using the barcode of the derivative.

Therefore, we modify the earlier characterization and propose the following two-step procedure to characterize the convexity (equivalently, concavity) of a function  $f$  on  $[-1, 1]$  using its first derivative  $f'$ :

- (i) First, compare the barcode of  $f'$  and  $-f'$ , qualitatively. In particular, compare the number of 0-dimensional features in the barcode of  $f'$  and  $-f'$ . If there are more than one 0-dimensional features in the barcode of  $f'$  or  $-f'$ , conclude that  $f$  is not convex (or concave). Otherwise, proceed with the following step.
- (ii) Characterize the convexity (concavity) of a function  $f$  on  $[-1, 1]$  by the fact that there exists a critical point of  $f$ , say,  $c \in [-1, 1]$  such that  $f$  is non-decreasing (non-increasing) on  $[c, 1]$  and non-increasing (non-decreasing) on  $[-1, c]$ .

In the above characterization, step (i) ensures that  $f'$  is monotone on  $[-1, 1]$  or not. Since any structure impeding the monotone structure of the derivative would result in the birth of new connected components in the barcodes of either  $f'$  or  $-f'$  making a qualitative difference in the barcodes of  $f'$  and  $-f'$ . This fact is evident from Figure 10 where the true barcode of  $m_1$  and  $-m_1$  are qualitatively different. On the other hand, step (ii) is required to characterize the convexity (concavity) without using the second derivative of the function. We use the characterization of monotonicity proposed in Section 5.1 to investigate the monotonicity of  $f$  on  $[-1, c]$  and  $[c, 1]$  in step (ii).

We infer the convexity of the function  $m$  aforementioned in this subsection and compare the results with the respective SiZer maps. To infer the convexity of  $m$  from the observed data, we need to consider the significant features in the observed barcode to apply step (i) of the proposed characterization. Note that, since we aim to infer the convexity of  $m$  on the entire domain  $[-1, 1]$ , the 0-dimensional feature with the largest persistence must be significant to proceed with step (ii), else we conclude that the observed structure is not convex (concave) significantly. The reason is that the features with shorter persistence represent structures in the subset of the domain  $[-1, 1]$  whereas here we need to infer the monotonicity of  $m_1$  on  $[-1, 1]$ . For example, it can be seen in Table 3 that the feature with shorter persistence  $[a_2, b_2]$  is significant with the

birth time  $b_2 < 0$  (see, Figure 9). This implies that the observed structure is significantly non-increasing (see, Section 5.1) in the local regions determined by their respective critical points. This fact can also be validated by the SiZer maps in Figure 12 wherein the critical points  $\hat{\mathbf{c}}_p$  corresponding to the observed features lie in red regions on the Sizer maps (see, Figure 12). This implies that the observed structure is significantly non-increasing in the local regions  $[-0.8, -0.6]$ ,  $[-0.6, -0.3]$ , and  $[-0.5, -0.2]$ , respectively, for  $n = 100, 150, 200$ . Recall that green dots on the SiZer maps highlight the critical points  $\hat{\mathbf{c}}_p$ , and the observed features in the estimated barcodes  $\mathcal{B} = \{[a_1, b_1], \dots, [a_p, b_p]\}$  are arranged in decreasing order of persistence.

We simulate noisy observations from  $m$  using the noise distribution as the normal distribution with mean 0 and variance 0.1, truncated at  $[-1, 1]$ . We take the bandwidth  $h = n^{-1/3}$  for  $n \in \{100, 150, 200\}$ . The true function ( $m$ ), the estimated function ( $\hat{m}$ ), the true derivative ( $m_1$ ), and the estimated derivative ( $\hat{m}_1$ ) are shown in Figure 9. It is evident from the visual inspection of the graph of  $m_1$  in Figure 9 that  $m_1$  is not a non-decreasing function implying that  $m$  is not convex. We aim to infer this fact from the observed data using the proposed characterization.

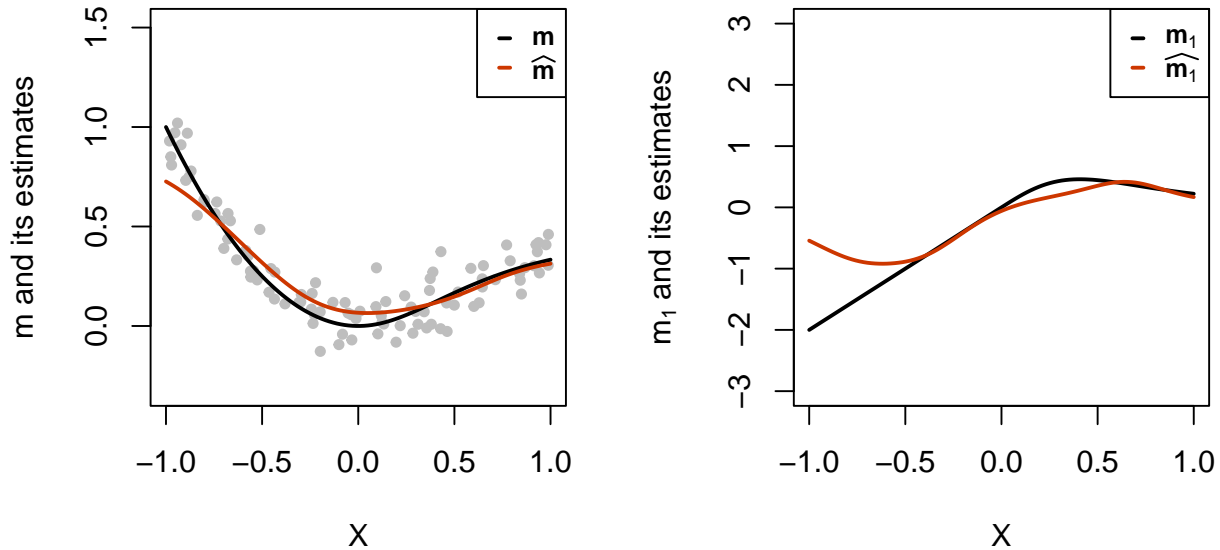


Figure 9: An illustrative example for investigating the convexity of a regression function.

We estimate  $m$  and  $m_1$  using the normal and Cauchy kernel supported on  $[-1, 1]$ . We compute barcodes using the procedure given in Section 3 for  $\hat{m}_1$  and  $-\hat{m}_1$  shown in Figure 10 and 11 for the normal and Cauchy kernel, respectively. It can be seen in Figure 10 and 11 that there are two 0-dimensional features in the observed barcode of  $m_1$  and  $-m_1$  for  $h = n^{-1/3}, n \in \{100, 150, 200\}$ . We need to assess the statistical significance of the observed features in the barcode to apply step (i) to infer the convexity of  $m$ .

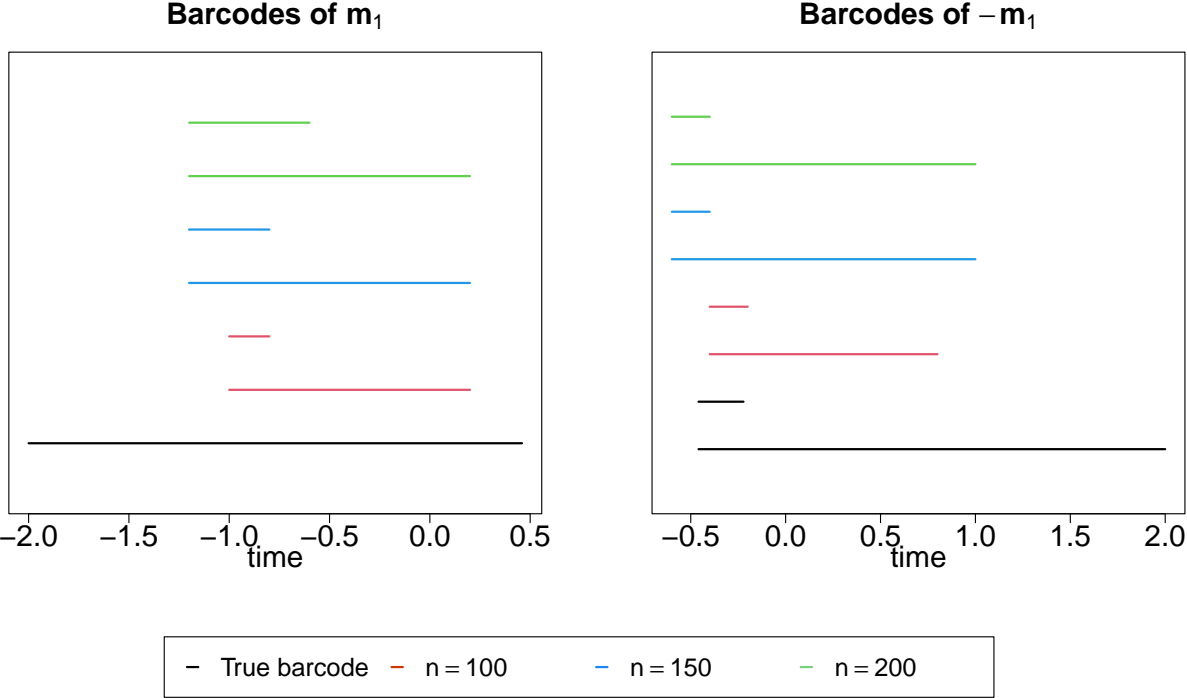


Figure 10: True and estimated barcodes of  $m_1$  and  $-m_1$  for  $n = 100, 150, 200$ .

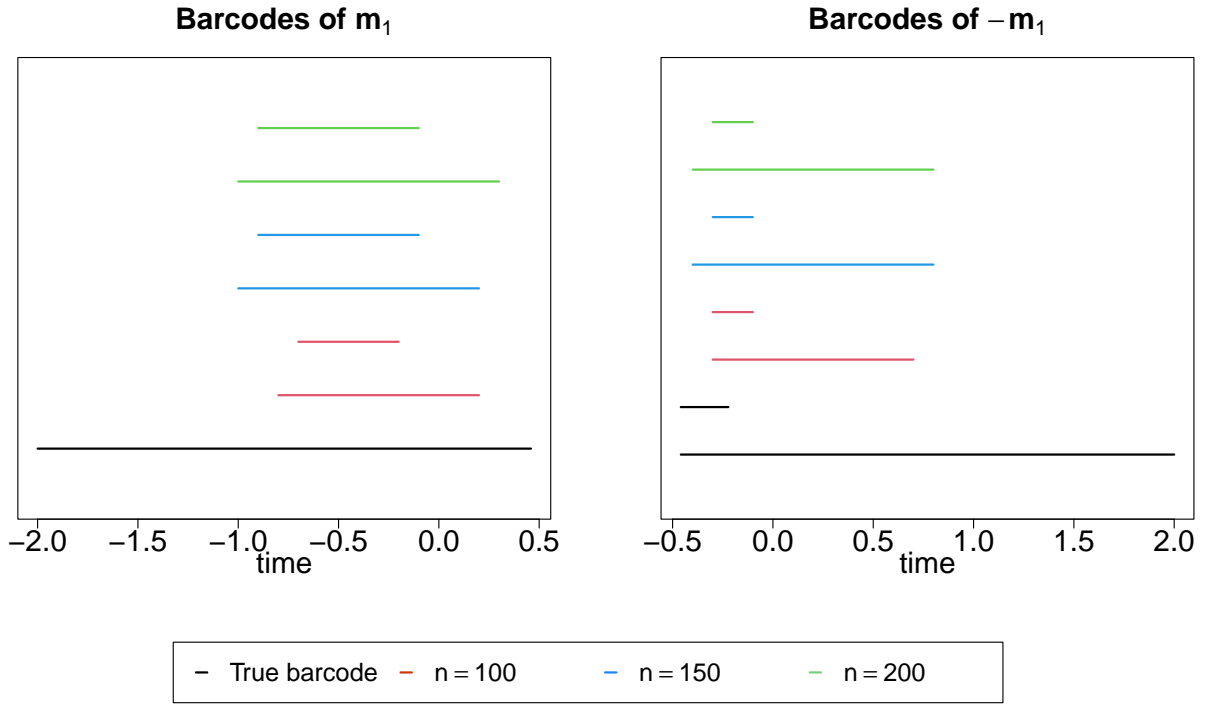


Figure 11: True and estimated barcodes of  $m_1$  and  $-m_1$  for Cauchy Kernel.

Now, we assess the statistical significance of these observed 0-dimensional features which is tabulated in Table 3, 4, 5, 6. It is evident from these tables that the observed 0-dimensional with the largest persistence is not significant for both  $\hat{m}_1$  and  $-\hat{m}_1$ . Therefore, we infer that the observed structure is not convex. The SiZer maps in Figure 12 also suggest that the observed structure is not convex. Since there is a purple region between the red and blue region for the bandwidth  $h = n^{-1/3}$  highlighted by the black dotted line. This suggests that the underlying function  $m$  is not convex.

Table 3: Significance of convexity for Gaussian Kernel.

	Barcode of $\hat{m}_1$											
	$n = 100$				$n = 150$				$n = 200$			
	$a_1$	$b_1$	$a_2$	$b_2$	$a_1$	$b_1$	$a_2$	$b_2$	$a_1$	$b_1$	$a_2$	$b_2$
$\hat{c}_p$	-0.6	0.2	-0.6	-0.8	-0.6	0.8	-0.6	-0.3	-0.5	0.1	-0.5	-0.2
$\hat{\beta}_1$	-3.5	0.8	-3.5	-1.3	-3.6	0.5	-3.6	-2.6	-3.6	0.3	-3.6	-2.2
p-value	$< 10^{-14}$	0.1	$< 10^{-14}$	0.007	$< 10^{-16}$	0.2	$< 10^{-16}$	$< 10^{-9}$	$< 10^{-16}$	0.4	$< 10^{-16}$	$< 10^{-6}$

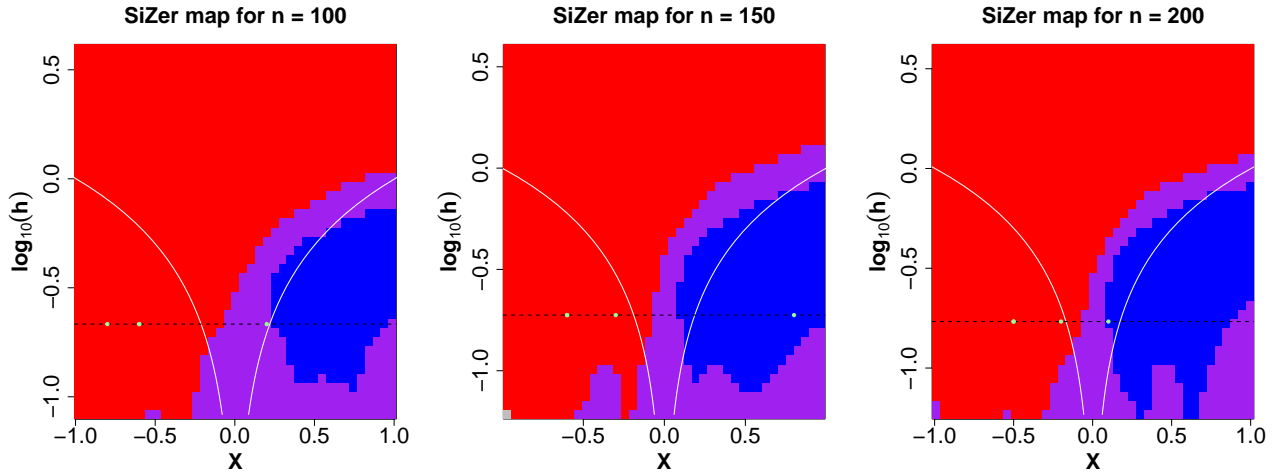


Figure 12: SiZer analysis of the regression function.

Table 4: Significance of convexity for  $-m_1$ .

	Barcode of $-\hat{m}_1$											
	$n = 100$				$n = 150$				$n = 200$			
	$a_1$	$b_1$	$a_2$	$b_2$	$a_1$	$b_1$	$a_2$	$b_2$	$a_1$	$b_1$	$a_2$	$b_2$
$\hat{c}_p$	0.4	0.8	0.4	0.7	0.5	-0.8	0.5	0.7	0.7	-0.8	0.7	0.8
$\hat{\beta}_1$	-1.4	0.6	-1.4	-0.6	-1.6	1.7	-1.6	-1.1	-1.2	1.9	-1.2	-1.1
p-value	<b>0.003</b>	0.2	<b>0.003</b>	0.2	<b>0.0005</b>	0.0003	<b>0.0005</b>	<b>0.01</b>	<b>0.003</b>	$< 10^{-5}$	<b>0.003</b>	<b>0.01</b>

Table 5: Significance of convexity for Cauchy Kernel.

	Barcode of $\hat{m}_1$											
	$n = 100$				$n = 150$				$n = 200$			
	$\mathbf{a}_1$	$\mathbf{b}_1$	$\mathbf{a}_2$	$\mathbf{b}_2$	$\mathbf{a}_1$	$\mathbf{b}_1$	$\mathbf{a}_2$	$\mathbf{b}_2$	$\mathbf{a}_1$	$\mathbf{b}_1$	$\mathbf{a}_2$	$\mathbf{b}_2$
$\hat{\mathbf{c}}_p$	-0.7	0.4	-0.5	-0.1	-0.7	0.4	-0.7	-0.07	-0.6	0.5	-0.5	-0.02
$\hat{\beta}_1$	-2.2	1.3	-3.1	-0.9	-2.7	1.4	-3.02	-0.5	-3.5	1.7	-3.7	-0.68
<b>p-value</b>	$< 10^{-6}$	0.02	$< 10^{-9}$	0.1	$< 10^{-8}$	0.01	$< 10^{-9}$	0.3	$< 10^{-13}$	0.003	$< 10^{-13}$	0.2

Table 6: Significance of convexity for Cauchy Kernel for  $-m_1$ .

	Barcode of $-\hat{m}_1$											
	$n = 100$				$n = 150$				$n = 200$			
	$\mathbf{a}_1$	$\mathbf{b}_1$	$\mathbf{a}_2$	$\mathbf{b}_2$	$\mathbf{a}_1$	$\mathbf{b}_1$	$\mathbf{a}_2$	$\mathbf{b}_2$	$\mathbf{a}_1$	$\mathbf{b}_1$	$\mathbf{a}_2$	$\mathbf{b}_2$
$\hat{\mathbf{c}}_p$	0.4	-0.5	0.4	0.8	0.4	-0.5	0.7	0.9	0.7	-0.8	0.8	0.1
$\hat{\beta}_1$	-1.3	3.3	-1.3	-0.4	-2.003	3.3	-1.1	-0.2	-1.3	0.9	-1.1	-0.2
<b>p-value</b>	<b>0.01</b>	$< 10^{-9}$	<b>0.01</b>	0.4	<b>0.0004</b>	$< 10^{-10}$	<b>0.02</b>	0.7	<b>0.005</b>	0.05	<b>0.02</b>	0.7

### 5.3 Modality

We provide an illustrative example to infer the modality of a smooth regression function from noisy samples using estimated barcodes of its first derivative. We characterize modes of a smooth regression function  $f$  on  $[-1, 1]$  using the critical points of  $f$ . We say that a critical point  $c \in [-1, 1]$  is a mode of  $f$  if there exists a  $\delta > 0$  such that  $f$  is concave in  $[c - \delta, c + \delta]$ . We use the method of zero crossings of the derivative to estimate the critical points.

We simulate noisy observations from the mixture of two normal distributions truncated on  $[-1, 1]$  with mean  $-0.5$  and  $0.5$ , with the same variance  $0.1$ , and equal mixture proportions. The graph of true and estimated function is given in Figure 13 along with the SiZer map of the data. We obtain critical points of the estimated function using significant zero crossings of the derivative. We focus on two of the critical points depicted by blue dots in Figure 13, and aim to infer the modality of the underlying true function in the local regions highlighted by green vertical dotted lines in Figure 13. These regions are  $\delta$ -neighbourhood around the critical points of the estimated function, where we choose  $\delta = 0.1$ . We use the aforementioned characterization to infer whether the critical points represent modes of the true function.

We obtain barcodes of the estimated derivative using the procedure given in Section 3, and infer the monotonicity of the function in the local regions  $[c - \delta, c]$  and  $[c, c + \delta]$  to infer modality. Note that, here  $c$  represents the critical points of interest, and  $\delta = 0.1$ . We denote the critical points of the estimated function  $\hat{m}$  depicted in Figure 13 by  $\hat{c}_1$  and  $\hat{c}_2$ . The estimated barcodes for the Gaussian kernel are shown in Figure 14 for the sample size  $n = 50$ , and the bandwidth  $h = n^{-1/3}$ . The estimated critical values  $\hat{c}_1$  and  $\hat{c}_2$  are **-0.47**, **0.51**, respectively. The estimated barcodes in the local regions  $[\hat{c}_1 - \delta, \hat{c}_1]$ ,  $[\hat{c}_1, \hat{c}_1 + \delta]$ ,  $[\hat{c}_2 - \delta, \hat{c}_2]$ ,  $[\hat{c}_2, \hat{c}_2 + \delta]$  are **{[0.05, 0.72]}**, **{[-0.72, 0.03]}**, **{[0.09, 0.81]}**, **{[-0.69, 0.07]}**, respectively, for  $\delta = 0.1$ . Note that, we highlight the true and estimated death or birth times in different regions using black and green dotted lines, respectively, to investigate monotonicity in these regions (see, Section 5.1). It is evident from the estimated barcodes of  $\hat{m}_1$  that  $\hat{m}$  is increasing on  $[\hat{c}_1 - 0.1, \hat{c}_1]$ , since the death time (0.05) of the observed feature is positive. On the other hand, the birth time of the feature in the estimated barcode on  $[\hat{c}_1, \hat{c}_1 + 0.1]$  is non-negative yielding that  $\hat{m}$  is

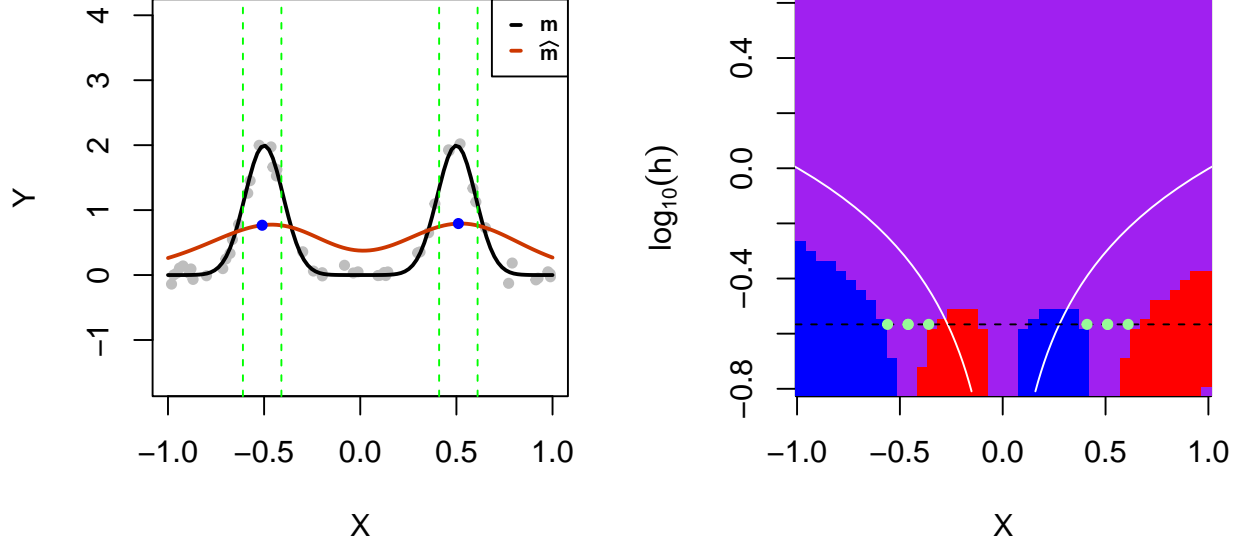


Figure 13: A bimodal function and its estimate along with the SiZer map of the observed data.

not non-increasing on  $[\hat{c}_1, \hat{c}_1 + 0.1]$ . Hence, we conclude that the critical point  $\hat{c}_1$  is not a mode of the estimated function. Similar conclusion also holds for  $\hat{c}_2$ . It can be seen from Table 7 that the observed critical points are not significant. This fact can be validated by the SiZer map of the data in Figure 13. Since for  $h = n^{-1/3}$  (black dotted line) there is a purple region between the two blue and red regions indicating that the observed critical points are not significant.

Table 7: Significance of modes for Gaussian Kernel.

	Barcode for $\hat{c}_1$				Barcode for $\hat{c}_2$			
	On $[\hat{c}_1 - 0.1, \hat{c}_1]$		On $[\hat{c}_1, \hat{c}_1 + 0.1]$		On $[\hat{c}_2 - 0.1, \hat{c}_2]$		On $[\hat{c}_2, \hat{c}_2 + 0.1]$	
	$\mathbf{a}_1$	$\mathbf{b}_1$	$\mathbf{a}_1$	$\mathbf{b}_1$	$\mathbf{a}_1$	$\mathbf{b}_1$	$\mathbf{a}_1$	$\mathbf{b}_1$
$\hat{c}_p$	-0.46	-0.56	-0.36	-0.46	0.51	0.41	0.61	0.51
$\hat{\beta}_1$	-0.27	2.6	-2.7	-0.39	-0.05	2.3	-2.2	-0.16
<b>p-value</b>	0.84	0.05	<b>0.02</b>	0.7	0.9	0.06	<b>0.04</b>	0.8

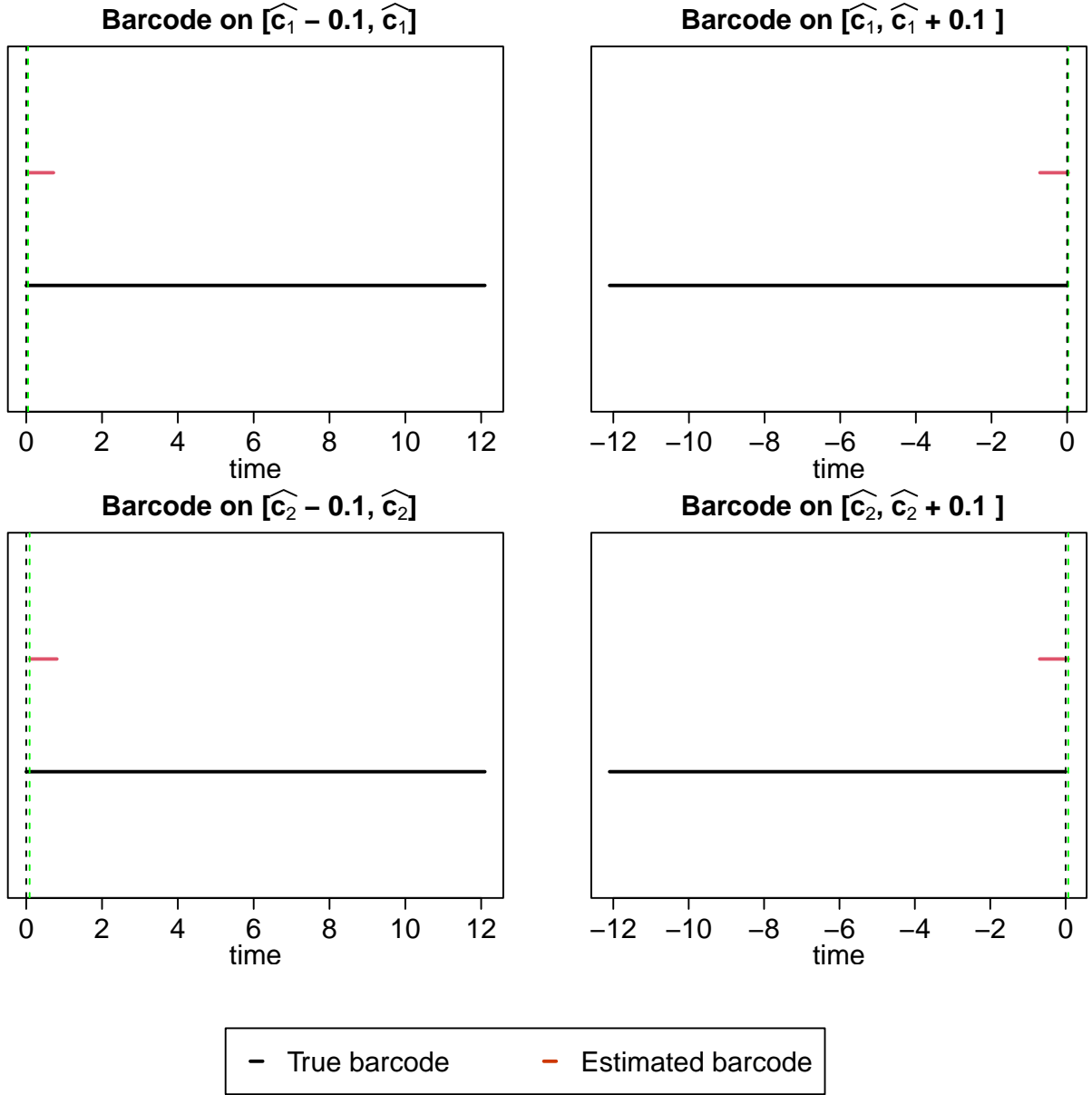


Figure 14: Estimated barcodes of  $\hat{m}_1$  for the Gaussian kernel for  $h = n^{-1/3}, n = 50$ .

Next, we obtain the barcodes of  $\hat{m}_1$  using the Cauchy kernel. The critical values to be investigated to identify modes are  $\hat{c}_1 = -0.51$  and  $\hat{c}_2 = 0.51$ . The estimated barcodes in the local regions  $[\hat{c}_1 - 0.1, \hat{c}_1], [\hat{c}_1, \hat{c}_1 + 0.1], [\hat{c}_2 - 0.1, \hat{c}_2], [\hat{c}_2, \hat{c}_2 + 0.1]$  are  $\{[0.3, 1.1]\}, \{[-0.7, 0.3]\}, \{[0.01, 0.91]\}, \{[-0.94, -0.02]\}$ , respectively. These barcodes are shown in Figure 15. It is evident from the estimated barcode that only  $\hat{c}_2$  can be characterized to be a

mode. However, it is not significant as can be seen in Table 8.

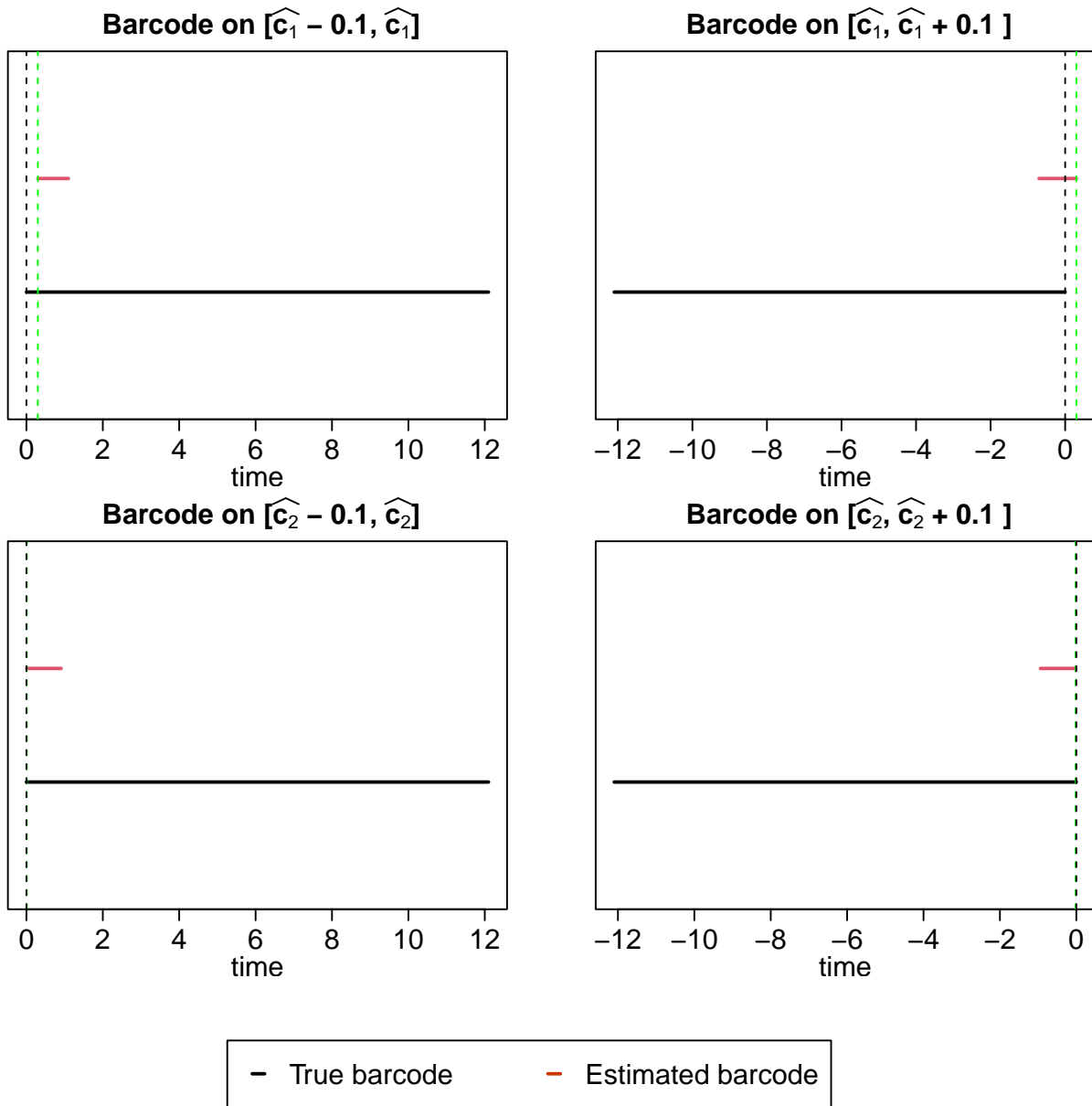


Figure 15: Estimated barcodes of  $\hat{m}_1$  for the Cauchy kernel for  $h = n^{-1/3}, n = 50$ .

Table 8: Significance of modes for Cauchy Kernel.

	Barcode for $\hat{c}_1$				Barcode for $\hat{c}_2$			
	On $[\hat{c}_1 - 0.1, \hat{c}_1]$		On $[\hat{c}_1, \hat{c}_1 + 0.1]$		On $[\hat{c}_2 - 0.1, \hat{c}_2]$		On $[\hat{c}_2, \hat{c}_2 + 0.1]$	
	$\mathbf{a}_1$	$\mathbf{b}_1$	$\mathbf{a}_1$	$\mathbf{b}_1$	$\mathbf{a}_1$	$\mathbf{b}_1$	$\mathbf{a}_1$	$\mathbf{b}_1$
$\hat{c}_p$	-0.51	-0.59	-0.41	-0.5	0.51	0.41	0.61	0.51
$\hat{\beta}_1$	1.4	4.7	-3.4	1.006	-0.47	3.3	-3.8	-0.6
<b>p-value</b>	0.3	0.0007	<b>0.01</b>	0.5	0.7	0.01	<b>0.002</b>	0.6

## 6 Real data study

We apply the proposed methodology to two real data sets to infer local structures such as monotonicity, convexity, and modality. We provide statistical significance of observed structures using the methodology proposed in Section 4, and compare the results with the respective SiZer maps. We investigate local structures in the first data set for two different bandwidths  $h_1, h_2$ , highlighted by black and gray horizontal dotted lines on the SiZer maps, respectively. On the other hand, we choose a bandwidth to observe a certain structure and investigate its significance for the second data set. In addition, we also focus on certain structures arising in certain local regions highlighted by green dotted lines in Figure 20. In this section, we use the Gaussian kernel supported on  $[-1, 1]$  to estimate the underlying true regression function.

### 6.1 Data set 1

We consider the intercountry lifecycle savings data available in the R software library, “datasets.” This data is based on the life-cycle savings hypothesis developed by Franco Modigliani (1975). According to the lifecycle savings hypothesis, the savings ratio (Y) (aggregate personal savings divided by disposable income) is explained by the following four variables: the percentage of the population less than 15 years old ( $X_1$ ), the percentage of the population over 75 years old ( $X_2$ ), the disposable income per capita ( $X_3$ ), and the percentage rate of change in per-capita

disposable income ( $X_4$ ). This data set consists of observations on these four variables for 50 countries. We fit a non-parametric regression model (see, Equation (3.1)) for each of the four regressors  $X_1, X_2, X_3, X_4$  to infer local structures. A non-parametric regression fit ( $\hat{m}$ ) for  $X_1$ , the estimated derivative ( $\hat{m}_1$ ), SiZer map for  $\hat{m}$ , and the estimated barcodes of  $\hat{m}_1$  for two different bandwidths,  $h_1 = 15, h_2 = 8$ , is shown in Figure 16. It is evident from the barcode of  $\hat{m}_1$  that  $\hat{m}$  is significantly decreasing for  $h_1$ , and (see, Figure 16). It can be seen in Table 9 that the observed monotone structure is significant at 5 % level of significance. Since the birth times of the 0-dimensional features in the estimated barcode of  $\hat{m}_1$  is negative for  $h_1$  (see, Figure 16) and significant (see, Table 9). However, for  $h_2 = 8$ , the birth times are negative but not significant implying that the observed structure is not significantly decreasing.

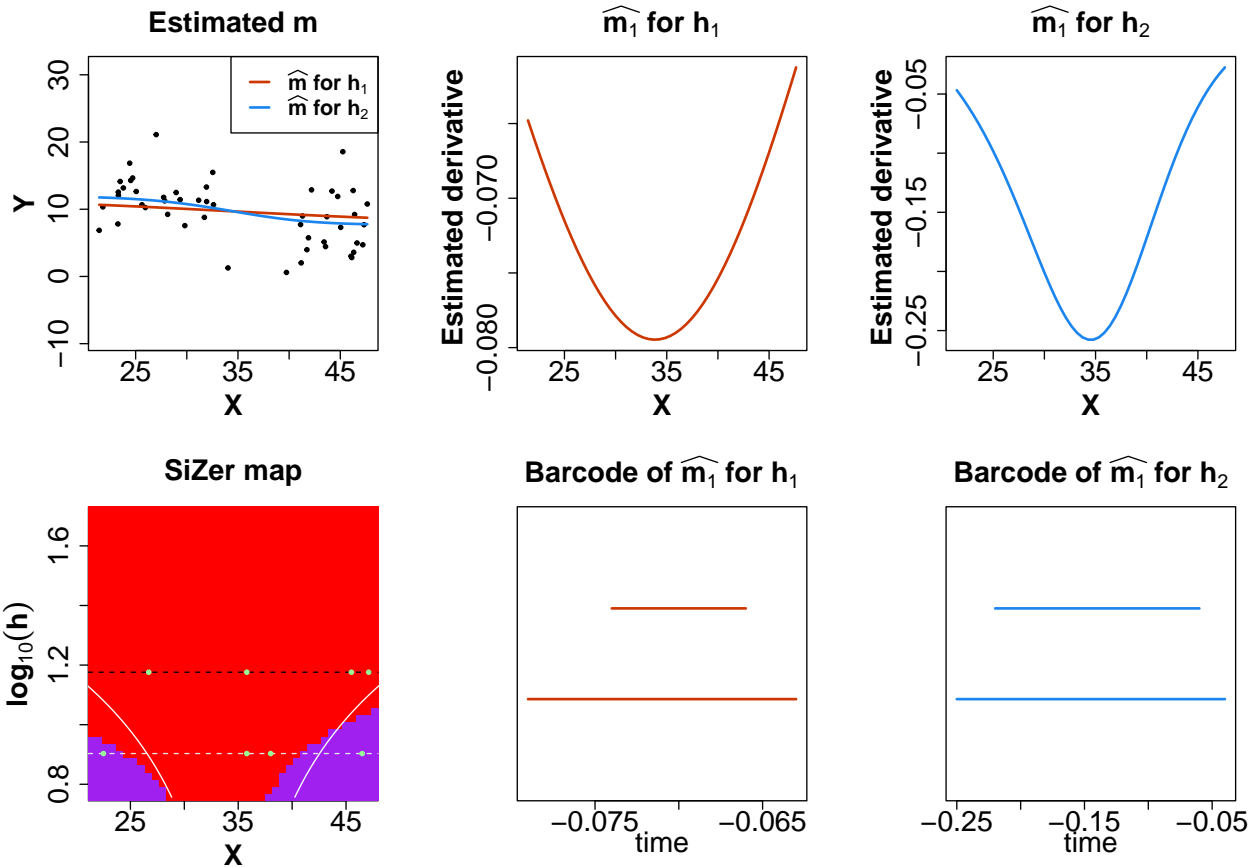


Figure 16: Comparison of local structures in the estimated regression function ( $\hat{m}$ ) derived from the estimated derivative ( $\hat{m}_1$ ) with the SiZer map for  $X_1$  using the bandwidths  $h_1 = 15, h_2 = 8$ .

Now, we compare the inferred monotone structure from the barcode of the estimated derivative with the SiZer map of the data. Note that, for  $h_1 = 15$  denoted by the black dotted line on the SiZer map in Figure 16, the observed structure is significantly decreasing as highlighted by the red region. The significance of features articulated in Table 9 suggests the same. Since the critical points, denoted by the green dots on the SiZer map, corresponding to the observed features lie on the red region on the SiZer map. This implies that function is significantly decreasing at these points. This further implies that  $\hat{m}_1$  at these points is significantly negative which is consistent with the results in Table 9. However, for  $h_2 = 8$ , denoted by the gray dotted line, the SiZer map indicates the purple region for some x-locations implying that the observed structure is not significantly decreasing. It can be seen in Table 9 that the observed birth times ( $b_1$ ) are not significant indicating that  $\hat{m}$  can not be concluded to be significantly decreasing.

Table 9: Significance of local structures for  $X_1$ .

	$h_1 = 15$				$h_2 = 8$			
	$a_1$	$b_1$	$a_2$	$b_2$	$a_1$	$b_1$	$a_2$	$b_2$
$\hat{c}_p$	35.8	47.1	26.7	45.5	35.8	46.5	38.01	22.5
$\hat{\beta}_1$	$-2.7 \times 10^3$	-3595.5	-3620.7	-3452.3	-926.8	1195.1	-854.8	946.3
<b>p-value</b>	<b>0.0005</b>	<b>0.0194</b>	<b>0.0006</b>	<b>0.006</b>	<b>0.0003</b>	0.05	<b>0.001</b>	0.05

Now, for the regressors  $X_2$ ,  $X_3$  and  $X_4$ , some key insights about the observed structure in  $\hat{m}$  are summarized as follows. The observed structure in  $\hat{m}$  is not significantly monotone for each of the bandwidths for  $X_2$  as suggested by the estimated barcodes in Figure 17 and Table 10. It can be seen in Table 10 that the observed features for  $h_1$  are not significant while for  $h_2$  the feature  $[a_1, b_1]$  is significant. Note that, for  $h_2$ ,  $a_1 < 0$  and  $b_1 > 0$  indicating that  $\hat{m}$  can not be a monotone function that is also evident from the SiZer map in Figure 17. However, for  $h_1$  the SiZer map suggests significantly increasing structure contrary to the structure derived from the estimate barcode in Table 10.

The observed barcode in Figure 18 indicates that  $\hat{m}$  is monotone increasing for the bandwidths  $h_1 = Q_X(0.95)$ , and  $h_2 = Q_X(0.75)$ , where  $Q_X(u)$ ,  $u \in (0, 1)$ , denote the  $u$ -th empirical quantile

of the underlying regressor  $X$  (in this case  $X_3$ ). However, the observed monotone structure is not significant for  $h_1$  whereas significant for  $h_2$  as evident from Table 11. In contrast, the SiZer map in Figure 18 indicates that the observed structure is not significantly monotone increasing. The observed barcode in Figure 19 indicates that  $\hat{m}$  is monotone increasing for the bandwidths  $h_1 = 25$ , and  $h_2 = Q_X(0.95)$ . However, the observed monotone structure is significant only for the bandwidth  $h_2 = Q_X(0.95)$ . In contrast, the SiZer map indicates that the observed monotone structure is significant for  $h_1$ , and insignificant for  $h_2$ .

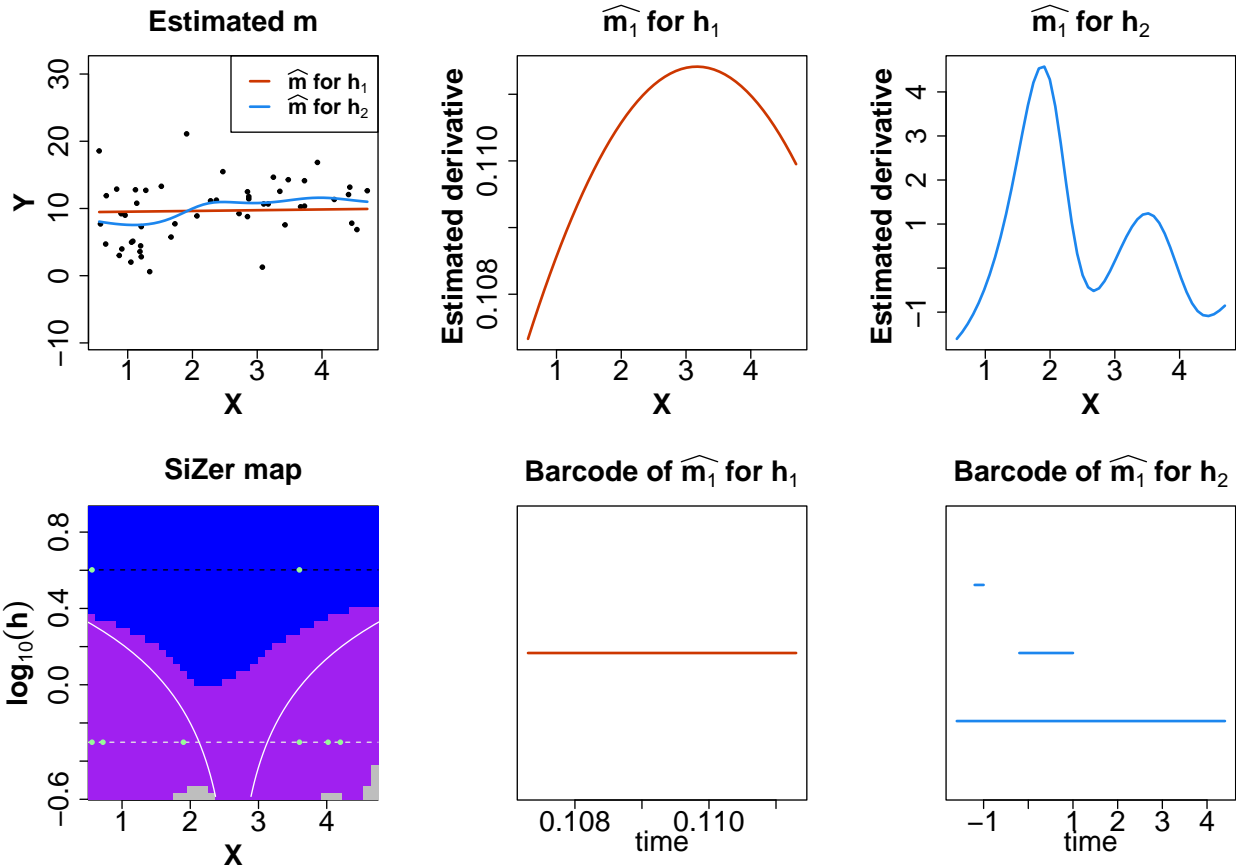


Figure 17: Comparison of local structures in the estimated regression function ( $\hat{m}$ ) derived from the estimated derivative ( $\hat{m}_1$ ) with the SiZer map for  $X_2$  using the bandwidths  $h_1 = 4$ ,  $h_2 = 0.5$ .

Table 10: Significance of local structures for  $X_2$ .

	$h_1 = 4$		$h_2 = 0.5$					
	$a_1$	$b_1$	$a_1$	$b_1$	$a_2$	$b_2$	$a_3$	$b_3$
$\hat{c}_p$	0.56	3.6	0.56	1.9	4.02	3.6	0.72	4.2
$\hat{\beta}_1$	1219.31	951.6	-58.4	28.4	-7.2	1.8	-64.09	-15.01
p-value	0.01	0.02	<b>0.0003</b>	<b>0.006</b>	0.51	0.8	<b>0.0009</b>	0.21

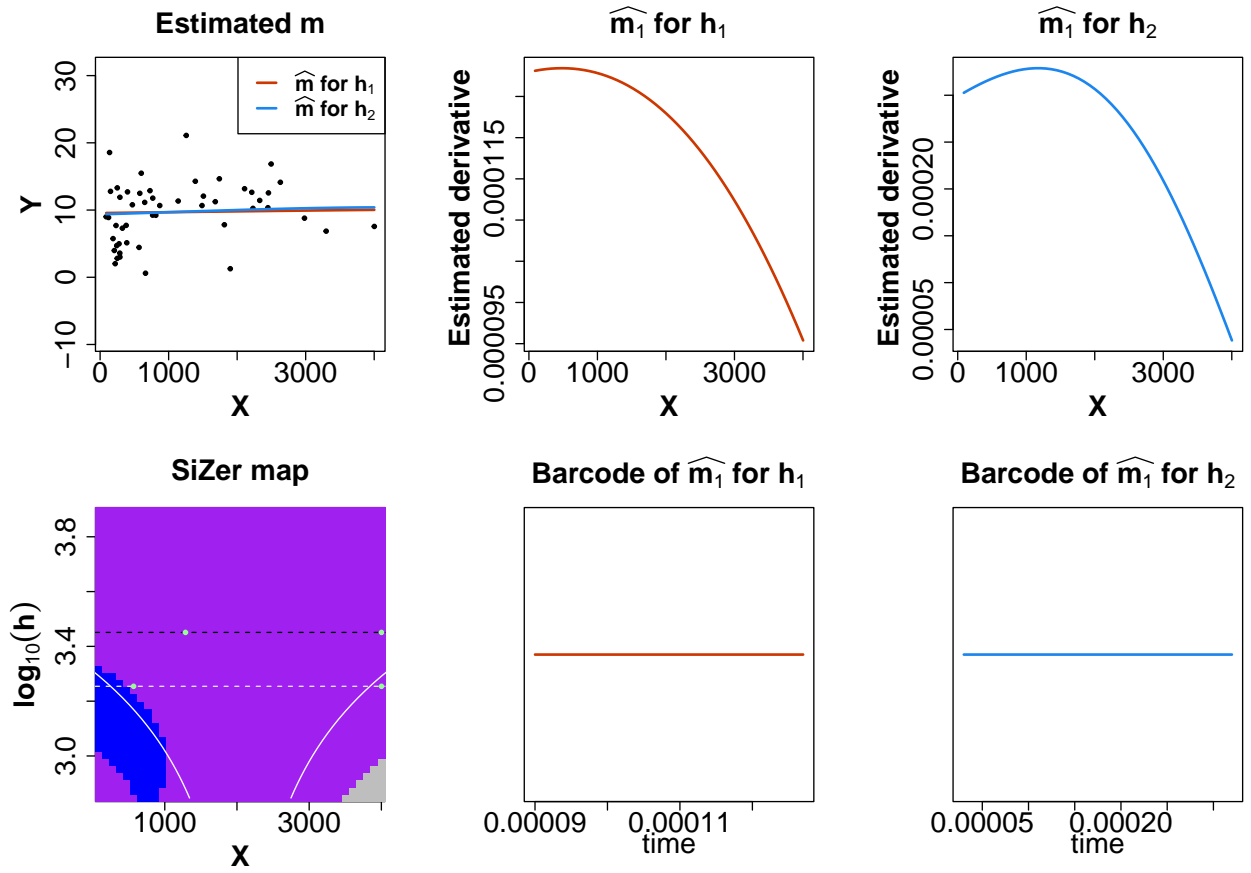


Figure 18: Comparison of local structures in the estimated regression function ( $\hat{m}$ ) derived from the estimated derivative ( $\hat{m}_1$ ) with the SiZer map for  $X_3$  using the bandwidths  $h_1 = Q_X(0.95)$ ,  $h_2 = Q_X(0.75)$ .

Table 11: Significance of local structures for  $X_3$  and  $X_4$

	Variable $X_3$				Variable $X_4$			
	$h_1 = Q_X(0.95)$		$h_2 = Q_X(0.75)$		$h_1 = 25$		$h_2 = Q_X(0.95)$	
	$a_1$	$b_1$	$a_1$	$b_1$	$a_1$	$b_1$	$a_1$	$b_1$
$\hat{c}_p$	4001.8	1286.7	4001.8	568.07	0.22	12.6	16.7	11.3
$\hat{\beta}_1$	$-2.7 \times 10^5$	$4.8 \times 10^5$	$-2.9 \times 10^5$	$3.6 \times 10^5$	18652.5	14418.6	-1977.6	544.5
p-value	0.6	0.08	<b>0.009</b>	0.01	0.01	0.04	<b>0.003</b>	0.56

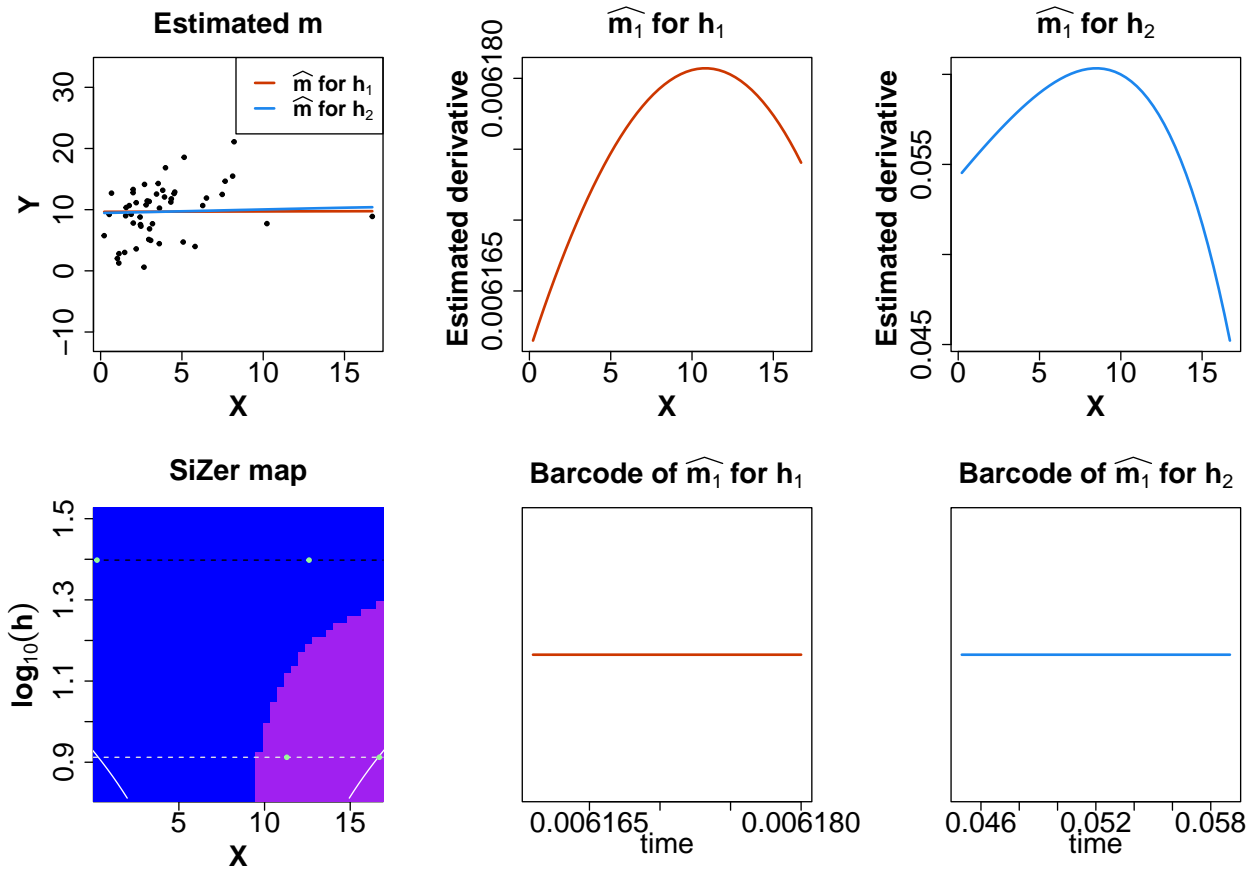


Figure 19: Comparison of local structures in the estimated regression function ( $\hat{m}$ ) derived from the estimated derivative ( $\hat{m}_1$ ) with the SiZer map for  $X_4$  using the bandwidths  $h_1 = 25$ ,  $h_2 = Q_X(0.95)$ .

## 6.2 Data set 2

We consider the “Motorcycle data” available in the R package “adlift”. This data set contains  $n = 133$  observations of simulations measuring the effects of motorcycle crashes on victims heads. There are two variables in the data set; time after a simulated impact with motorcycles (X) and head acceleration of a post-mortem human test object (Y). The observed structure in the data set is shown in Figure 20. We fit a non-parametric regression model (see, Equation 3.1) to the observed data, and aim to infer the observed structure using the proposed methodology. We compute the barcode of the estimated derivative using the procedure given in Section 3 to investigate if the observed structure is significant or not. In addition, we aim to investigate if the valley structure arising in the region  $[15, 25]$ , and the observed peak in the the region  $[25, 35]$  is significant or not. These local regions are highlighted via green vertical dotted lines in Figure 20.

A non-parametric regression fit ( $\hat{m}$ ), the estimated derivative ( $\hat{m}_1$ ), the SiZer map for  $\hat{m}$ , and the estimated barcodes of  $\hat{m}_1$  is shown in Figure 20. We choose the bandwidth  $h = 2.5$  highlighted by the black dotted line on the SiZer map, to estimate the regression function  $m$ . It is evident from Table 12 that none of the observed features in the barcode of  $\hat{m}_1$  are significant. Hence, the observed structure in the data is not significant, which is also evident from the SiZer map in Figure 20. Furthermore, the observed valley in  $[15, 25]$  and the observed peak in  $[25, 35]$  are not significant, since from Table 13 none of the features in the observed barcode in  $[15, 25]$  and  $[25, 35]$  are significant. Note that, the same inference is also drawn from the SiZer map as there is a purple region between the red and blue region on  $[15, 25]$ , and a purple region after the blue region on  $[25, 35]$ . This suggests that the observed peak and valley in the region  $[25, 35]$  and  $[15, 25]$ , respectively, is not significant.

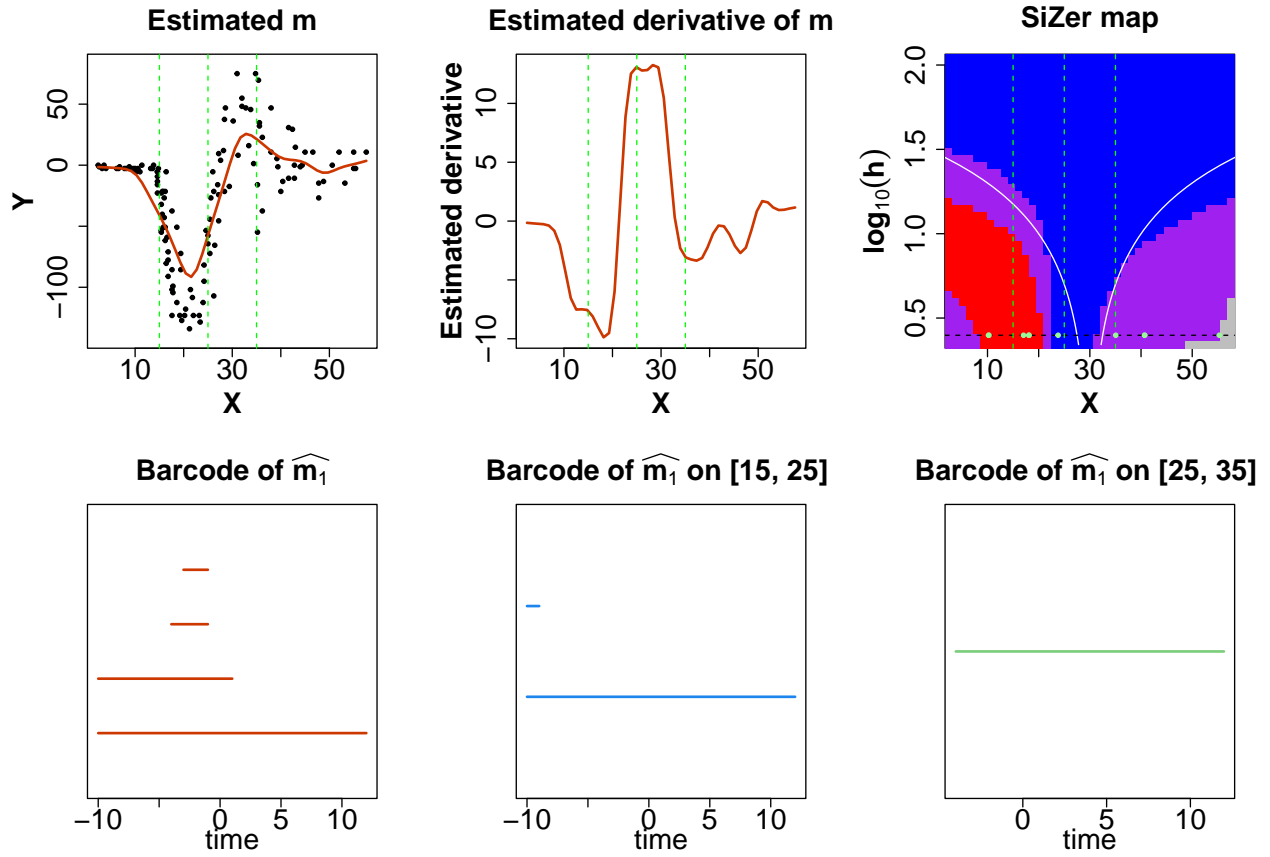


Figure 20: Comparison of local structures in the estimated regression function ( $\hat{m}$ ) derived from the estimated derivative ( $\hat{m}_1$ ) with the SiZer map using the bandwidths  $h = 2.5$

Table 12: Significance of the observed local structures for  $h = 2.5$

	$\mathbf{a}_1$	$\mathbf{b}_1$	$\mathbf{a}_2$	$\mathbf{b}_2$	$\mathbf{a}_3$	$\mathbf{b}_3$	$\mathbf{a}_4$	$\mathbf{b}_4$
$\hat{c}_p$	18.1	23.8	18.1	55.3	10.2	40.7	35.06	40.7
$\hat{\beta}_1$	-2485.8	3434.2	-2485.8	-236.1	-578.6	-238.01	-1438.9	-238.01
<b>p-value</b>	<b>0.0305</b>	0.0001	<b>0.0305</b>	0.675	0.468	0.733	0.119	0.733

Table 13: Significance of convexity on  $[15, 25]$ , and modality on  $[25, 35]$ .

	Convexity on $[15, 25]$				Modality on $[25, 35]$	
	$\mathbf{a_1}$	$\mathbf{b_1}$	$\mathbf{a_2}$	$\mathbf{b_2}$	$\mathbf{a_1}$	$\mathbf{b_1}$
$\hat{\mathbf{c}}_p$	18.1	23.8	18.1	17.04	10.2	23.8
$\hat{\mathbf{\beta}}_1$	-2485.8	3434.2	-2485.8	-5679.01	-578.6	3434.2
<b>p-value</b>	<b>0.0305</b>	0.0001	<b>0.0305</b>	$\mathbf{1.8 \times 10^{-5}}$	0.468	0.0001

## 7 Conclusion

In this article, we explored structures such as monotonicity, convexity, and modality in smooth regression curves via persistent homology of the super-level sets of a particular function. That particular function is the first derivative of the regression function. In general, persistent homology can be applied to identify structures in level sets of functions in terms of connected components and holes. We exploit the fact that derivatives of a function carry important geometric information about the function; therefore, one can identify useful structures in a function by investigating the persistent homology of its derivatives. The main problem that impedes one from using persistent homology to explore the geometric properties of a function via its derivative is the consistency of the estimates of persistent homology of its derivatives. The problem of consistency for the estimates of persistent homology arises due to the non-availability of an estimator of the derivative of the function that converges uniformly. Therefore, the usual procedure for estimating the persistent homology is ruled out in this case.

However, [1] proposed a different procedure based on the kernel estimation of statistical functions (density and regression functions), applicable in the present context. We apply this procedure to estimate the persistent homology of the first derivative of regression functions and establish its consistency. This procedure is useful in the present context since its consistency does not require uniform convergence of the estimator of the underlying function. Thus, this procedure paves the way for exploring structures via the persistent homology of the first derivative of the regression functions. For future considerations, it would be tempting to extend

this procedure for higher-order derivatives to explore some stimulating structures in regression curves. We would also like to explore the possibility of extending this procedure for the gradient of the regression function when there is more than one regressor. In this context, we would like to discuss the possibility of extending the procedure when there is more than one regressor and the difficulties involved therein. Note that when there is more than one regressor, the regression function is  $m : \mathbb{R}^d \rightarrow \mathbb{R}, d \geq 2$ . In this case, the first derivative, that is the gradient of the function, will be a function  $m_1 : \mathbb{R}^d \rightarrow \mathbb{R}^d, d \geq 2$ . The usual persistent homology, also called one-parameter persistent homology, tracks the evolution of homological features in nested sequences of topological spaces indexed by a parameter  $t \in \mathcal{I} \subset \mathbb{R}$ . For example, filtrations built on point cloud usually have a radius  $r \geq 0$  of Euclidean balls, or in super level-set filtrations, usually, it is the height of a real-valued function that varies over  $\mathbb{R}$ . Therefore, the usual persistent homology can be used only for real-valued functions. In contrast, here we aim to compute the persistent homology of a vector-valued function that does not have the usual notion of height. Thus, to compute persistent homology for the first derivative of a function when the domain of the function is  $\mathbb{R}^d, d \geq 2$ , we have to resort to the so-called, multiparameter persistent homology. The multiparameter persistent homology is meant to track the evolution of topological features for filtrations of the form  $\{\mathcal{X}_t; \mathbf{t} \in \mathbb{R}^d, \}, d \geq 2$ . However, it does not have a straightforward extension of one-parameter persistent homology because it does not have a nice numerical invariant such as barcode. Thus, though it provides some information about the underlying topological space, it is not a compact numerical invariant, making it restrictive for topological inference. For these reasons, it is not so straightforward to make topological inferences about the derivative of the regression function when there is more than one regressor.

## 8 Appendix

### 8.1 Notations

- $a_n \asymp b_n$  denotes  $\lim_{n \rightarrow \infty} a_n/b_n = 1$ .
- $K_h(x) = K(\frac{x}{h})$ , for any  $x \in S$ ,  $S$  is the support of the Kernel function  $K$ .

- $K^2(x) \triangleq (K(x))^2$ , for any  $x \in S$ .
- $\lceil x \rceil$  denotes the smallest integer larger than or equal to  $x$ .
- $\mathbb{B}_h(x)$  denotes a Ball of radius  $h$  centered around the point  $x$ .
- $\mathcal{X}_n = \{(X_i, Y_i); i = 1, \dots, n\}$
- $\partial A$  denotes the boundary of set  $A$ .
- $\partial D_t(h) \triangleq \bigcup_{x \in \partial D_t} \mathbb{B}_h(x)$  where  $D_t$  denotes super level set at the level  $t$ .
- $D_t^+(h) \triangleq D_t \cup \partial D_t(h)$  and  $D_t^-(h) \triangleq D_t \setminus \partial D_t(h)$ .

## 8.2 Definitions

**Definition 8.1 (Hoeffding's inequality)** Let  $Z_1, \dots, Z_n$  be independent random variables such that  $\mathbb{E}(Z_i) = 0$ , and there exists constants  $a_i < b_i$  such that  $\mathbb{P}(Z_i \in [a_i, b_i]) = 1$  for all  $i = 1, \dots, n$ . Then for all  $u > 0$ , we have

$$\mathbb{P}\left(\sum_{i=1}^n Z_i \geq u\right) \leq \exp\left(\frac{-2u^2}{\sum_{i=1}^n (b_i - a_i)^2}\right).$$

## 8.3 Proof of Theorem 3.1

First, we state and prove the following two lemmas that will be used to prove the Theorem 3.1. Then we provide proof of the Theorem 3.1. The Lemma 8.1 and Lemma 8.2 can be interpreted as follows. First, recall the set  $\mathcal{X}_n^t \triangleq \{X_i : \hat{f}_n(X_i) \geq t, i = 1, \dots, n\}$  in step 2 of the described procedure. Note that even small errors in the estimator  $\hat{f}_n$  may result in a false positive or false negative error in the assignments of data points to  $\mathcal{X}_n^t$  with respect to the super-level set that corresponds to the true function  $m_1$ . The true super-level set is denoted as  $D_t$  here. A tiny error in  $\mathcal{X}_n^t$  may introduce large errors in the estimated persistent homology of  $D_t$ . Therefore we need to find the probability of false positive and false negative assignments of data points to the set  $\mathcal{X}_n^t$  with respect to  $D_t$ . We find an upper bound of false positive and false negative

errors by inflating and deflating the set  $D_t$  by a radius  $h$ . In other words, we define the two sets  $D_t^+(h)$  and  $D_t^-(h)$  as follows. First, we define the tube of radius of  $h$  around the boundary of  $D_t$ , That is

$$\partial D_t(h) \triangleq \bigcup_{x \in \partial D_t} \mathbb{B}_h(x), \partial D_t \text{ is boundary of } D_t.$$

Then define the following sets:

$$D_t^+(h) \triangleq D_t \cup \partial D_t(h) \text{ and } D_t^-(h) \triangleq D_t \setminus \partial D_t(h),$$

where  $D_t^+(h)$  and  $D_t^-(h)$  corresponds to inflating and deflating the set  $D_t$  by a radius  $h$ , respectively. The Lemma 8.1 computes upper bounds for false positive and false negative errors of assignments of data points to the set  $\mathcal{X}_n^t$ . Then using the Lemma 8.1, Lemma 8.2 shows that the set  $\hat{D}_t(n, h)$  (See, Equation 3.4) is sandwiched between two non-random approximations of  $D_t$  with high probability.

**Lemma 8.1** *Under the assumptions (A.1)-(A.5) and (B.1)-(B.5), for every  $t > 0$  and  $\epsilon \in (0, t)$ , if  $h \equiv h(n) \rightarrow 0$  as  $n \rightarrow \infty$  such that  $nh^2 \rightarrow \infty$ , then there exists a constant  $C_\epsilon$  such that for large enough  $n$  we have*

$$\mathbb{P}(\exists X_i \in \mathcal{X}_n^t | X_i \notin D_{t-\epsilon}^+(h)) \leq ne^{-C_\epsilon nh^2} \quad (8.1)$$

and

$$\mathbb{P}(\exists X_i \notin \mathcal{X}_n^t | X_i \in D_{t+\epsilon}^-(h)) \leq ne^{-C_\epsilon nh^2}, \quad (8.2)$$

where  $D_t^+(h) \triangleq D_t \cup \partial D_t(h)$ ,  $D_t^-(h) \triangleq D_t \setminus \partial D_t(h)$  and  $\partial D_t(h) \triangleq \bigcup_{x \in \partial D_t} \mathbb{B}_h(x)$ .

**Proof:** First, recall that the set  $\mathcal{X}_n^t = \{X_i : \hat{m}_{1,n}(X_i) \geq t\}$ , where  $\hat{m}_{1,n}$  is defined in

Equation 3.9. Then we start the proof by proving Equation 8.1. Consider the probability

$$\begin{aligned}
\mathbb{P}(\exists X_i \in \mathcal{X}_n^t | X_i \notin D_{t-\epsilon}^+(h)) &= \bigcup_{i=1}^n \mathbb{P}(X_i \in \mathcal{X}_n^t | X_i \notin D_{t-\epsilon}^+(h)) \\
&\leq n \mathbb{P}(X_1 \in \mathcal{X}_n^t | X_1 \notin D_{t-\epsilon}^+(h)) \\
&= n \mathbb{P}(X_1 \in \mathcal{X}_n^t | X_1 \in (D_{t-\epsilon}^+(h))^c) \\
&= n \mathbb{P}(\hat{m}_{1,n}(X_1) \geq t | X_1 \in (D_{t-\epsilon}^+(h))^c) \\
&= n \int_{(D_{t-\epsilon}^+(h))^c} \int_{\mathbb{R}} f(x, y) \mathbb{P}(\hat{m}_{1,n}(X_1) \geq t | X_1 = x, Y_1 = y) dy dx.
\end{aligned} \tag{E.2}$$

Now, we shall use the strong consistency of the Nadaraya-Watson estimator of  $m$ , denoted as  $\hat{m}_n$ . We have

$$\begin{aligned}
\hat{m}_{1,n}(x) &= \frac{\sum_{i=1}^n K_{1,h}(x - X_i) Y_i}{\sum_{i=1}^n K_h(x - X_i)} - \frac{\sum_{i=1}^n K_{1,h}(x - X_i) \hat{m}_n(x)}{\sum_{i=1}^n K_h(x - X_i)} \\
&\asymp \frac{\sum_{i=1}^n K_{1,h}(x - X_i) (Y_i - m(x))}{\sum_{i=1}^n K_h(x - X_i)} \text{ almost surely,}
\end{aligned} \tag{E.3}$$

where E.3 follows from the fact that  $\hat{m}_n(x) \asymp m(x)$  almost surely for all  $x \in \mathbb{R}$ .

Now, consider the probability

$$\begin{aligned}
\mathbb{P}[\hat{m}_{1,n}(X_1) \geq t | X_1 = x, Y_1 = y] &= \mathbb{P} \left[ \frac{\sum_{i=1}^n K_{1,h}(X_1 - X_i) (Y_i - \hat{m}_n(X_1))}{\sum_{i=1}^n K_h(X_1 - X_i)} \geq t | X_1 = x, Y_1 = y \right] \\
&\asymp \mathbb{P} \left[ \frac{\sum_{i=1}^n K_{1,h}(X_1 - X_i) (Y_i - m(X_1))}{\sum_{i=1}^n K_h(X_1 - X_i)} \geq t | X_1 = x, Y_1 = y \right] \\
&\hspace{20em} \text{(Using \a href{#}{E.3})} \\
&= \mathbb{P} \left[ \sum_{i=2}^n \{K_{1,h}(x - X_i) (Y_i - m(x)) - tK_h(x - X_i)\} \geq t \right] \\
&\leq \mathbb{P} \left[ \sum_{i=2}^n (Z_i - \mathbb{E}(Z_i)) \geq t - \sum_{i=2}^n \mathbb{E}(Z_i) \right] \\
&\lesssim \mathbb{P} \left[ \sum_{i=2}^n (Z_i - \mathbb{E}(Z_i)) \geq t + \epsilon \delta p_{\min} 2(n-1)h \right], \tag{E.4}
\end{aligned}$$

where

$$Z_i = K_{1,h}(x - X_i) (Y_i - m(x)) - (m_1(X_i) + \epsilon)K_h(x - X_i). \tag{8.3}$$

We have defined  $Z_i$  using the fact that since  $X_i \notin D_{t-\epsilon}^+(h)$  this implies that  $m_1(X_i) \leq t - \epsilon$ , and the inequality in Equation  follows from the Result .

Now, we would like to apply Hoeffding's inequality (See Definition ) for the random variables  $Z_i - \mathbb{E}Z_i, i = 2, \dots, n$ , therefore consider the following:

1. We have  $\mathbb{E}[Z_i - \mathbb{E}Z_i] = 0$ , and  $Z_i - \mathbb{E}Z_i$ 's are independent, since  $(X_i, Y_i)$ 's are independent for all  $i = 2, \dots, n$ .
2. We have  $|Z_i| \leq \tau (Y_{\max} + M) + (M_1 + \epsilon)$

Therefore, using 1 and 2 above, and applying Hoeffding's inequality for  $u = t + \epsilon \delta p_{\min} 2(n -$

1)  $h$ , we have

$$\begin{aligned}
\mathbb{P}[\hat{m}_{1,n}(X_1) \geq t | X_1 = x, Y_1 = y] &\leq \exp \frac{-2(t + \epsilon \delta p_{min} 2(n-1)h)^2}{4(n-1)[\tau(Y_{max} + M) + (M_1 + \epsilon)]^2} \\
&= \exp \frac{-n^2 h^2 \left(\frac{t}{nh} + \epsilon \delta p_{min} 2 \frac{(n-1)}{n}\right)^2}{2(n-1)[\tau(Y_{max} + M) + (M_1 + \epsilon)]^2} \\
&\asymp \exp \frac{-nh^2 2\epsilon^2 \delta^2 p_{min}^2}{[\tau(Y_{max} + M) + (M_1 + \epsilon)]^2} \\
&= \exp(-nh^2 C_\epsilon), \tag{E.5}
\end{aligned}$$

where  $C_\epsilon$  is a constant depending on  $\epsilon$ , defined as

$$C_\epsilon = \frac{2\epsilon^2 \delta^2 p_{min}^2}{[\tau(Y_{max} + M) + (M_1 + \epsilon)]^2}. \tag{8.4}$$

Now, using the Equation E.5 in the Equation E.2 we have

$$\begin{aligned}
\mathbb{P}(\exists X_i \in \mathcal{X}_n^t | X_i \notin D_{t-\epsilon}^+(h)) &\leq n \int_{(D_{t-\epsilon}^+(h))^c} \int_{\mathbb{R}} f(x, y) \exp(-nh^2 C_\epsilon) dy dx \\
&= n \exp(-nh^2 C_\epsilon) \int_{\mathbb{R}} \int_{\mathbb{R}} f(x, y) dy dx \\
&= n e^{-nh^2 C_\epsilon}
\end{aligned}$$

This completes the proof of inequality in Equation 8.1. To prove the inequality in 8.2, we proceed in the same way using the fact that  $X_i \in D_{t+\epsilon}^-(h)$  implies that  $m_1(X_i) \geq t + \epsilon$ , and define random variables  $Z_i^*$  as

$$Z_i^* = (m_1(X_i) - \epsilon) K_h(x - X_i) - K_{1,h}(x - X_i) (Y_i - m(x)).$$

Now, observe that similar to Result 8.1, we will have same result for  $\mathbb{E}[Z_i^*]$ , thus similar to Equation E.4, we have

$$\mathbb{P}[\hat{m}_{1,n}(X_1) \leq t | X_1 = x, Y_1 = y] \leq \mathbb{P}\left[\sum_{i=2}^n (Z_i^* - \mathbb{E}[Z_i^*]) \geq \epsilon \delta p_{min} 2(n-1)h - t\right].$$

Then apply Hoeffding's inequality for random variables  $Z_i^* - \mathbb{E}[Z_i^*]$  and proceed in the same way to get the Equation E.5 and, from E.5, it is easy to prove the inequality in Equation 8.2.

This completes the proof of the Lemma 8.1. □

**Lemma 8.2** *Under the assumptions (A.1)-(A.5) and (B.1)-(B.5), for every  $t > 0$ , and  $\epsilon \in (0, t)$  if  $h \equiv h(n) \rightarrow 0$  as  $n \rightarrow \infty$  such that  $nh^2 \rightarrow \infty$ , then for large enough  $n$ , we have*

$$\mathbb{P}(D_{t+\epsilon}^-(2h) \subset \hat{D}_t(n, h) \subset D_{t-\epsilon}^+(2h)) \geq 1 - 3ne^{-C_\epsilon nh^2}. \quad (8.5)$$

**Proof:** Let  $E_1$  and  $E_2$  denotes the following events respectively,

$$D_{t+\epsilon}^-(2h) \subset \hat{D}_t(n, h) \text{ and } \hat{D}_t(n, h) \subset D_{t-\epsilon}^+(2h).$$

Then, the probability in Equation 8.5 can be written as:

$$\mathbb{P}(E_1 \cap E_2) = 1 - \mathbb{P}(E_1^c \cup E_2^c) \geq 1 - \mathbb{P}(E_1^c) - \mathbb{P}(E_2^c). \quad (8.6)$$

Now, since  $\hat{D}_t(n, h) \supset \mathcal{X}_n^t$ , using the Lemma 8.1 we have

$$\begin{aligned} \mathbb{P}(E_2^c) &= \mathbb{P}\left(\hat{D}_t(n, h) \not\subset D_{t-\epsilon}^+(2h)\right) = \mathbb{P}\left(\hat{D}_t(n, h) \subset (D_{t-\epsilon}^+(2h))^c\right) \\ &\leq \mathbb{P}\left(\mathcal{X}_n^t \cap (D_{t-\epsilon}^+(h))^c \neq \emptyset\right) \leq ne^{-nh^2 C_\epsilon}. \end{aligned} \quad (E.6)$$

Now, consider the probability,

$$\mathbb{P}(E_1^c) = \mathbb{P}\left(D_{t+\epsilon}^-(2h) \not\subset \hat{D}_t(n, h)\right) = \mathbb{P}\left(\exists S \subset D_{t+\epsilon}^-(2h) : S \cap \hat{D}_t(n, h) = \emptyset\right). \quad (8.7)$$

Note that in view of the fact that  $m_1$  is bounded,  $D_{t+\epsilon}^-(2h)$  is bounded, hence it can be covered by finitely many subsets from it. Let  $\gamma \in (0, 1)$  and define a cover of  $D_{t+\epsilon}^-(2h)$  as  $\{\mathbb{B}_{\gamma h}(u) : u \in \mathcal{I}\}$ , where  $\mathcal{I} \subset D_{t+\epsilon}^-(2h)$  is a finite index set. Then for all  $x \in D_{t+\epsilon}^-(2h)$  there exists a  $u \in \mathcal{I}$  such that  $|x - u| \leq \gamma h$ . By the construction of  $\hat{D}_t(n, h)$ , if  $x \notin \hat{D}_t(n, h)$  then  $x \notin \mathbb{B}_h(X_i)$  for all  $X_i \in \mathcal{X}_n^t$ .

Therefore, for any  $x \in S \subset D_{t+\epsilon}^-(2h)$ , where  $S$  satisfies that  $S \cap \hat{D}_t(n, h) = \emptyset$ , there exists a  $u \in \mathcal{I}$  such that  $|x - u| > (1 - \gamma)h$ . This implies that for any  $x \in D_{t+\epsilon}^-(2h)$  such that  $x \notin \hat{D}_t(n, h)$  there exists a  $u \in \mathcal{I}$  such that  $\mathbb{B}_{(1-\gamma)h}(u) \cap \hat{D}_t(n, h) = \emptyset$ .

Thus, the probability in Equation 8.7 can be written as

$$\begin{aligned} \mathbb{P}(E_1^c) &= \mathbb{P}\left(\exists u \in \mathcal{I} : \mathbb{B}_{(1-\gamma)h}(u) \cap \hat{D}_t(n, h) = \emptyset\right) \\ &\leq \mathbb{P}\left(\exists u \in \mathcal{I} : \mathbb{B}_{(1-\gamma)h}(u) \cap \mathcal{X}_n^t = \emptyset\right), \end{aligned} \quad (E.7)$$

where the Equation E.7 follows from the fact that  $\mathcal{X}_n^t \subset \hat{D}_t(n, h)$ . Now, note that there could be points in  $\mathcal{X}_n^t$ , that are added due to the error in the estimator  $\hat{m}_{1,n}$ , therefore probability in the Equation E.7 can be written as

$$\begin{aligned}
\mathbb{P}(E_1^c) &\leq \mathbb{P}(\exists u \in \mathcal{I} : \mathbb{B}_{(1-\gamma)h}(u) \cap \mathcal{X}_n^t = \emptyset) \\
&= \mathbb{P}(\exists u \in \mathcal{I} : \mathbb{B}_{(1-\gamma)h}(u) \cap \mathcal{X}_n^t = \emptyset; D_{t+\epsilon}^-(h) \cap \mathcal{X}_n \subset \mathcal{X}_n^t) \\
&\quad + \mathbb{P}(\exists u \in \mathcal{I} : \mathbb{B}_{(1-\gamma)h}(u) \cap \mathcal{X}_n^t = \emptyset; D_{t+\epsilon}^-(h) \cap \mathcal{X}_n \not\subset \mathcal{X}_n^t) \\
&\leq \mathbb{P}(\exists u \in \mathcal{I} : \mathbb{B}_{(1-\gamma)h}(u) \cap \mathcal{X}_n^t = \emptyset) + \mathbb{P}(D_{t+\epsilon}^-(h) \cap \mathcal{X}_n \not\subset \mathcal{X}_n^t). \tag{E.8}
\end{aligned}$$

Now, consider the following:

$$\begin{aligned}
\mathbb{P}(\exists u \in \mathcal{I} : \mathbb{B}_{(1-\gamma)h}(u) \cap \mathcal{X}_n^t = \emptyset) &= \sum_{u \in \mathcal{I}} \mathbb{P}(\mathbb{B}_{(1-\gamma)h}(u) \cap \mathcal{X}_n = \emptyset) \\
&= \sum_{u \in \mathcal{I}} \mathbb{P}(X_i \notin \mathbb{B}_{(1-\gamma)h}(u) \text{ for all } i \in \mathcal{X}_n) \\
&= \sum_{u \in \mathcal{I}} (1 - F_X(\mathbb{B}_{(1-\gamma)h}(u)))^n \\
&\leq \sum_{u \in \mathcal{I}} e^{-nF_X(\mathbb{B}_{(1-\gamma)h}(u))}, \tag{E.9}
\end{aligned}$$

where  $F_X$  is the distribution function of the regressors. Then, for  $0 < h < 1$ , we have

$$F_X(\mathbb{B}_{(1-\gamma)h}(u)) = \int_{u-(1-\gamma)h}^{u+(1-\gamma)h} p(x)dx \geq 2(1-\gamma)hp_{min} \geq 2(1-\gamma)h^2p_{min} \tag{8.8}$$

Also, note that since  $\mathcal{I}$  is a finite set that is there exist finitely many intervals of length  $2\gamma h$  that cover the set  $D_{t+\epsilon}^-(h)$ . This implies that there exists a positive number  $N_\gamma$  such that  $|\mathcal{I}| \leq N_\gamma 2\gamma h$ . Now using this fact with Equation 8.8 in Equation E.9, we have

$$\mathbb{P}(\exists u \in \mathcal{I} : \mathbb{B}_{(1-\gamma)h}(u) \cap \mathcal{X}_n^t = \emptyset) \leq N_\gamma 2\gamma h e^{-n2(1-\gamma)h^2p_{min}} = N_\gamma 2\gamma h e^{-nh^2C_\gamma}, \tag{8.9}$$

where  $C_\gamma = 2(1-\gamma)p_{min}$ . Now, note that the second term in Equation E.8 can be bounded by Lemma 8.1. Therefore, using the Equation 8.2, we have the following bound for the second term of Equation E.8,

$$\mathbb{P}(D_{t+\epsilon}^-(h) \cap \mathcal{X}_n \not\subset \mathcal{X}_n^t) \leq ne^{-C_\epsilon nh^2} \tag{8.10}$$

Now, using Equation 8.9 and Equation 8.10 in the Equation E.8, we have

$$\mathbb{P}(E_1^c) \leq N_\gamma 2\gamma h e^{-nh^2 C_\gamma} + n e^{-C_\epsilon n h^2} \leq 2n e^{-C_\epsilon n h^2}, \quad (8.11)$$

where the last inequality follows from the observation that  $C_\epsilon < C_\gamma$ , and for large  $n$ ,  $N_\gamma 2\gamma h \leq n$ .

Thus, using Equation 8.11 and Equation E.6 in Equation 8.6, we get the desired inequality as in Equation 8.5. This completes the proof of Lemma 8.2.  $\square$

### Proof of Theorem 3.1:

Let  $PH_k^\epsilon(m_1)$  denotes the persistent homology of the filtration  $\mathcal{D}^\epsilon$  defined as

$$\mathcal{D}^\epsilon \triangleq \{D_{t_i+\epsilon}\}_{i \in \mathbb{Z}}, \text{ where } t_{max} = 2\epsilon N_\epsilon, t_i = t_{max} - 2i\epsilon, \text{ and } N_\epsilon = \sup_{x \in \mathbb{R}} \lceil m_1(x)/2\epsilon \rceil.$$

Since  $\mathcal{D}^\epsilon$  is a discrete approximation of the continuous filtration  $\mathcal{D}$  with step size  $2\epsilon$ , therefore we have the maximum difference between  $PH_k(m_1)$  and  $PH_k^\epsilon(m_1)$  to be  $2\epsilon$ . That is, we have

$$\delta_B(PH_k(m_1), PH_k^\epsilon(m_1)) \leq 2\epsilon \quad (8.12)$$

Therefore, it is enough to prove that  $\delta_B(\widehat{PH}_k^\epsilon(m_1), PH_k^\epsilon(m_1)) \leq 3\epsilon$  holds with high probability. Let  $E$  be the event that the following sequence of inclusions holds:

$$D_{t_0+\epsilon} \hookrightarrow \hat{D}_{t_0}(n, h) \hookrightarrow D_{t_1+\epsilon} \hookrightarrow \hat{D}_{t_1}(n, h) \hookrightarrow D_{t_2+\epsilon} \hookrightarrow \dots$$

Now, applying Lemma 8.2  $N_\epsilon$  times for  $\hat{D}_{t_i}(n, h)$ , we have

$$\mathbb{P}(E) \geq 1 - 3nN_\epsilon e^{-C_{\epsilon/2} n h^2}$$

Therefore,  $\mathcal{D}^\epsilon$  and  $\hat{\mathcal{D}}^\epsilon$  are weakly  $\epsilon$ -interleaving. (See Definition 4.1 [7]). Now, using the weak stability theorem ([7]), we have

$$\delta_B(\widehat{PH}_k^\epsilon(m_1), PH_k^\epsilon(m_1)) \leq 3\epsilon. \quad (8.13)$$

Thus, from Equation 8.12 and Equation 8.13 we have

$$\delta_B(\widehat{PH}_k^\epsilon(m_1), PH_k(m_1)) \leq 5\epsilon.$$

Let  $E_1$  denotes the event that  $\delta_B(\widehat{PH}_k^\epsilon(m_1), PH_k(m_1)) \leq 5\epsilon$  then since  $E \subset E_1$  we have

$$\mathbb{P}\left(\delta_B(\widehat{PH}_k^\epsilon(m_1), PH_k(m_1)) \leq 5\epsilon\right) \geq 1 - 3nN_\epsilon e^{-C_{\epsilon/2} n h^2}.$$

This completes the proof.  $\square$

## 8.4 Some Auxiliary Results

**Result 8.1** For the random variable  $Z_i$  defined in the Equation 8.3, for large enough  $n$  such that  $h \equiv h(n)$  is sufficiently small, then we have  $\mathbb{E}[Z_i] \lesssim -\epsilon\delta p_{min}2h$ .

**Proof:** Consider the following:

$$\begin{aligned}
\mathbb{E}[Z_i] &= \mathbb{E}_{X_i} [K_{1,h}(x - X_i) \mathbb{E}_{Y_i|X_i}(Y_i - m(x))] - \mathbb{E}_{X_i} [(m_1(X_i) + \epsilon) K_h(x - X_i)] \\
&= \int_{x-\tau h}^{x+\tau h} K_{1,h}(x - \xi) (m(\xi) - m(x)) p(\xi) d\xi - \int_{x-h}^{x+h} (m_1(\xi) + \epsilon) K_h(x - \xi) p(\xi) d\xi \\
&\leq p_{max} (M - m(x)) \int_{x-\tau h}^{x+\tau h} K_{1,h}(x - \xi) d\xi - \delta p_{min} \int_{x-h}^{x+h} m_1(\xi) d\xi - \epsilon\delta p_{min} 2h \\
&= p_{max} (M - m(x)) [K_h(-\tau h) - K_h(\tau h)] - \delta p_{min} [m(x+h) - m(x-h)] - \epsilon\delta p_{min} 2h \\
&= -\delta p_{min} [m(x+h) - m(x-h)] - \epsilon\delta p_{min} 2h \quad (\text{By Assumption (A.2)}) \\
&\approx -\epsilon\delta p_{min} 2h,
\end{aligned}$$

where the last line follows from assuming that for small enough  $h$ , we have  $m(x+h) \approx m(x-h)$ .

□

**Acknowledgment :** The authors thank the editor, an anonymous associate editor, and two anonymous reviewers for their excellent comments and constructive criticisms, which significantly improve the article. Moreover, Subhra Sankar Dhar gratefully acknowledges his core research grant (Grant Number: CRG/2022/001489), the Government of India.

**Code availability:** The codes are available to the first author upon request.

## References

- [1] Bobrowski, O., Mukherjee, S., and Taylor, J. E. (2017). Topological consistency via kernel estimation. *Bernoulli*, 23(1):288 – 328.
- [2] Bubenik, P., Carlsson, G., Kim, P., and Luo, Z.-M. (2010). Statistical topology via morse theory persistence and nonparametric estimation. *Algebraic methods in statistics and probability II. Contemporary Mathematics.*, 516:75–92.

- [3] Carlsson, G. (2009). Topology and data. *American Mathematical Society*, 46:255–308.
- [4] Carlsson, G. (2014). Topological pattern recognition for point cloud data. *Acta Numerica*, 30:289–368.
- [5] Carlsson, G. and Vejdemo-Johansson, M. (2021). *Shape of Data*, page 94–144. Cambridge University Press.
- [6] Chaudhuri, P. and Marron, J. S. (1999). Sizer for exploration of structures in curves. *Journal of the American Statistical Association*, 94(447):807–823.
- [7] Chazal, F., Cohen-Steiner, D., Glisse, M., Guibas, L. J., and Oudot, S. Y. (2009). Proximity of persistence modules and their diagrams. In *Proceedings of the Twenty-Fifth Annual Symposium on Computational Geometry*, SCG '09, page 237–246, New York, NY, USA. Association for Computing Machinery.
- [8] Chazal, F., Guibas, L. J., Oudot, S. Y., and Skraba, P. (2011). Scalar field analysis over point cloud data. *Discrete & Computational Geometry*, 46(4):743–775.
- [9] Chazal, F., Guibas, L. J., Oudot, S. Y., and Skraba, P. (2013). Persistence-based clustering in riemannian manifolds. *J. ACM*, 60(6).
- [10] Chung, M. K., Bubenik, P., and Kim, P. T. (2009). Persistence diagrams of cortical surface data. In Prince, J. L., Pham, D. L., and Myers, K. J., editors, *Information Processing in Medical Imaging*, pages 386–397, Berlin, Heidelberg. Springer Berlin Heidelberg.
- [11] Cohen-Steiner, D., Edelsbrunner, H., and Harer, J. (2007). Stability of persistence diagrams. *Discrete & Computational Geometry*, 37(1):103–120.
- [12] Collins, A., Zomorodian, A., Carlsson, G., and Guibas, L. J. (2004). A barcode shape descriptor for curve point cloud data. *Computers & Graphics*, 28:881–894.
- [13] Cuevas, A. (1990). On pattern analysis in the non-convex case. *Kybernetes*, 19(6):26–33.
- [14] Cuevas, A., Febrero, M., and Fraiman, R. (2000). Estimating the number of clusters. *Canadian Journal of Statistics*, 28(2):367–382.

- [15] Cuevas, A. and Fraiman, R. (1997). A plug-in approach to support estimation. *The Annals of Statistics*, 25(6):2300 – 2312.
- [16] Dai, W., Tong, T., and Genton, M. G. (2016). Optimal estimation of derivatives in nonparametric regression. *Journal of Machine Learning Research*, 17(164):1–25.
- [17] De Brabanter, K., De Brabanter, J., De Moor, B., and Gijbels, I. (2013). Derivative estimation with local polynomial fitting. *J. Mach. Learn. Res.*, 14(1):281–301.
- [18] Dette, H., Dhar, S. S., and Wu, W. (2021). Identifying shifts between two regression curves. *Annals of the Institute of Statistical Mathematics*, 73(5):855–889.
- [19] Devroye, L. and Wise, G. L. (1980). Detection of abnormal behavior via nonparametric estimation of the support. *SIAM Journal on Applied Mathematics*, 38(3):480–488.
- [20] Dhar, S. S. and Wu, W. (2023). Comparing time varying regression quantiles under shift invariance. *Bernoulli*, 29(2):1527 – 1554.
- [21] Edelsbrunner, H. and Harer, J. (2008). Persistent homology—a survey. *Contemporary Mathematics 453*, 26:257–282.
- [22] Edelsbrunner, H. and Harer, J. (2010). *Computational Topology: An Introduction*. American Mathematical Society Providence, RI.
- [23] Fasy, B. T., Lecci, F., Rinaldo, A., Wasserman, L., Balakrishnan, S., and Singh, A. (2014). Confidence sets for persistence diagrams. *The Annals of Statistics*, 42(6):2301 – 2339.
- [24] Gasser, T. and Müller, H.-G. (1984). Estimating regression functions and their derivatives by the kernel method. *Scandinavian Journal of Statistics*, 11(3):171–185.
- [25] Ghrist, R. (2008). Barcodes: The persistent topology of data. *American Mathematical Society (New Series)*, 45:61–75.
- [26] Hartigan, J. (1975). *Clustering Algorithms*. Out-of-print Books on demand. Wiley.
- [27] Hatcher, A. (2002). *Algebraic topology*. Cambridge University Press, Cambridge.

- [28] Heckman, N. and Zamar, R. (2000). Comparing the shapes of regression functions. *Biometrika*, 87(1):135–144.
- [29] Munkres, J. (1984). *Elements of Algebraic Topology*. Westview Press; 1st edition.
- [30] Müller, D. W. and Sawitzki, G. (1991). Excess mass estimates and tests for multimodality. *Journal of the American Statistical Association*, 86(415):738–746.
- [31] Noda, K. (1976). Estimation of a regression function by the parzen kernel-type density estimators. *Annals of the Institute of Statistical Mathematics*, 28(1):221–234.
- [32] Park, C., Hannig, J., and Kang, K.-H. (2014). Nonparametric comparison of multiple regression curves in scale-space. *Journal of Computational and Graphical Statistics*, 23(3):657–677.
- [33] Park, C. and Kang, K.-H. (2008). Sizer analysis for the comparison of regression curves. *Computational Statistics & Data Analysis*, 52(8):3954–3970.
- [34] Phillips, J. M., Wang, B., and Zheng, Y. (2015). Geometric Inference on Kernel Density Estimates. In Arge, L. and Pach, J., editors, *31st International Symposium on Computational Geometry (SoCG 2015)*, volume 34 of *Leibniz International Proceedings in Informatics (LIPIcs)*, pages 857–871, Dagstuhl, Germany. Schloss Dagstuhl–Leibniz-Zentrum fuer Informatik.
- [35] Silverman, B. W. (1986). *Density Estimation for Statistics and Data Analysis*. Number 26 in Monographs on Statistics and Applied Probability. Chapman & Hall, London.
- [36] Tsybakov, A. B. (1997). On nonparametric estimation of density level sets. *The Annals of Statistics*, 25(3):948 – 969.
- [37] Zomorodian, A. and Carlsson, G. (2005). Computing persistent homology. *Discrete Comput. Geom.*, 33(2):249–274.